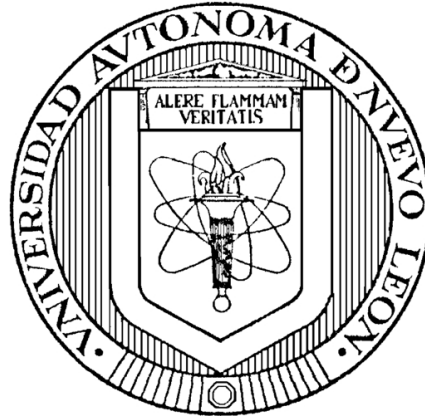


UNIVERSIDAD AUTÓNOMA DE NUEVO LEÓN
FACULTAD DE INGENIERÍA MECÁNICA Y ELÉCTRICA
DEPARTAMENT OF ELECTRICAL ENGINEERING



INSTANTANEOUS ESTIMATION OF OSCILLATING PHASORS
WITH TAYLOR^K-KALMAN-FOURIER FILTERS

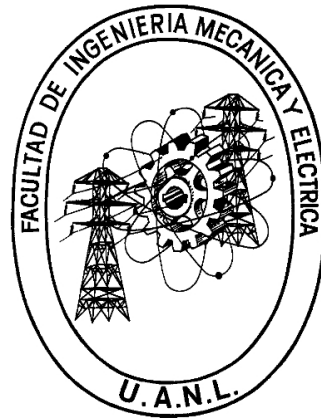
BY
JOHNNY RODRÍGUEZ MALDONADO

THESIS
FOR THE DEGREE OF DOCTOR IN ELECTRICAL
ENGINEERING

SAN NICOLÁS DE LOS GARZA, N.L.

AUG 2011

UNIVERSIDAD AUTÓNOMA DE NUEVO LEÓN
FACULTAD DE INGENIERÍA MECÁNICA Y ELÉCTRICA
DEPARTAMENT OF ELECTRICAL ENGINEERING



INSTANTANEOUS ESTIMATION OF OSCILLATING PHASORS
WITH TAYLOR^K-KALMAN-FOURIER FILTERS

BY
JOHNNY RODRÍGUEZ MALDONADO

THESIS
FOR THE DEGREE OF DOCTOR IN ELECTRICAL
ENGINEERING

SAN NICOLÁS DE LOS GARZA, N.L.

AUG 2011

UNIVERSIDAD AUTÓNOMA DE NUEVO LEÓN
FACULTAD DE INGENIERÍA MECÁNICA Y ELÉCTRICA
DEPARTAMENT OF ELECTRICAL ENGINEERING

The members of this committee recommend the thesis "**Instantaneous Estimation of Oscillating Phasors with Taylor^K-Kalman-Fourier Filters**" by **Johnny Rodríguez Maldonado**, student number: **1505411**, be accepted for its defense in fulfillment of the requirements for the degree of **Doctor in Electrical Engineering**.

Thesis Committee



Advisor

Dr. José Antonio de la O Serna



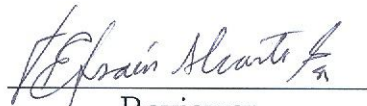
Reviewer

Dr. Carlos Manuel Astorga Zaragoza



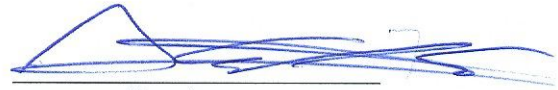
Reviewer

Dr. Juan Manuel Ramírez Arredondo



Reviewer

Dr. Efraín Alcorta García



Reviewer

Dr. Arturo Conde Enríquez



Vo. Bo.

Dr. Moisés Hinojosa Rivera
Division of Graduate Studies

San Nicolás de los Garza, N.L.

Aug 2011

To

Andrés, Antonia, Remy, Jesús, and Mariana L.

Acknowledgments

For achieving this project, many people were necessary that somehow contributed, and without whom it never would succeed.

Thanks to my advisor, Professor José A. de la O Serna, for giving me the opportunity to work with him, and the inspiration to drive it to completion. My reviewer professors: Carlos Manuel Astorga Zaragoza, Juan Manuel Ramírez Arredondo, Efraín Alcorta García and Arturo Conde Enríquez.

Thanks to my family: my parents, Andrés and Antonia, my sister Mariana L. and my brothers Remy and Jesús, all provided unconditional love and support.

Thanks to all of the students of the electrical department, for the nice spirit of collaboration.

Finally Special thanks to *Conacyt* for its economic support through the project I0013-90230: “Comparison of phasor estimation techniques under the optimization theory.”

Abstract

Instantaneous Estimation of Oscillating Phasors with Taylor^K-Kalman-Fourier Filters

Publication No. _____

Johnny Rodríguez Maldonado

Universidad Autónoma de Nuevo León

Facultad de Ingeniería Mecánica y Eléctrica

Advisor: Dr. José Antonio de la O Serna

Aug 2011

One of the most common phasor estimation techniques used nowadays is the one-cycle Fourier filter which estimate the phasor as the fundamental Fourier coefficient of the digital Fourier transform (DFT). It achieve exact estimates and has full harmonic rejection with steady-state input signals. But its phasor estimates are always delayed because it corresponds to the implementation of a symmetric finite impulse response (FIR) filter. The Kalman filter was also proposed in the eighties assuming also a static signal model (constant amplitude, frequency and phase) for the input voltage or current signals. At that time, it was demonstrated that it was equivalent to the Fourier filter and was quickly abandoned in the literature. In this work, we propose to extend the static signal model to a dynamic one, in which amplitude, frequency and phase are represented by band limited time functions. A Taylor approximation to those dynamic functions provides a state transition matrix that can be used in the Kalman algorithm. As the state vector contains the instantaneous first derivatives of the dynamic phasor, this signal model allows to estimate not only the dynamic phasor but also its first derivatives. The Taylor signal model together with the Kalman algorithm lead us to the Taylor^K-Kalman filter. Given the model, the traditional Kalman filter of the eighties corresponds to the Taylor⁰-Kalman filter, And by extending its state transition matrix to each

harmonic frequency, we arrive to the Taylor^K-Kalman-Fourier filter which offer an alternative to calculate the digital Fourier transform, but with causal infinite impulse response (IIR) filters. This means that its estimates are instantaneous (no delay at all), with much less infiltrated harmonic errors, as compared with the FFT estimates, and reducing the computational complexity.

The main contribution of this thesis is to have found the state-transition matrix of a state space dynamic signal model corresponding to the K -th order Taylor approximation to a power oscillation signal. With these transition matrices, the Kalman filter algorithm can be applied to find observers able to estimate the dynamic phasor and its first derivatives. The estimates obtained through this technique, are not only synchronous but also instantaneous, which is an important attribute for control applications. They also provide frequency estimates. The new filters reduce the total vector error achieved with the traditional Kalman filter; are much more stable, with settling times five times lower; and improve the phasor estimates of oscillations with frequency offset.

On the other hand one of the anomalies of the differentiators implemented with linear-phase finite impulse response (FIR) filters is their constant delay. Control applications require instantaneous estimates. Here we present a new family of derivative estimators referred to as *Taylor^K-Kalman filters*. They achieve ideal differentiator gains about the fundamental frequency for $K \geq 2$. By including the half sampling frequency component, their high sideband gain is mitigated, leading to low-pass (LP) filters. But the best gain reduction is obtained when the signal model incorporates the whole set of harmonic frequencies, obtaining the *Taylor^K-Kalman-Fourier differentiators*, which are able to estimate the derivatives of the complex envelope at each harmonic frequency. They preserve the ideal differentiator gain not only in the fundamental frequency, but also at each included harmonic frequency. When the spectral load of the input signal falls under the ideal operation bands, they operate as ideal differentiators, mapping the signal into its derivatives, making a Taylor-Fourier decomposition. But their main advantage is they provide instantaneous derivative estimates, very useful for control applications.

With the new *Taylor^K-Kalman(T^K - K) filters* for $K \geq 2$ are able to form a zero-flat phase response around the fundamental frequency, and to produce instantaneous oscillating phasor estimates. The frequency response of the zeroth and second order filters are established and illustrated. Their high sensitivity to noise lead us to design

more robust filters referred to as Taylor^K-Kalman-Fourier, because they incorporate the whole set of harmonics in their signal model. The bank of comb filters achieved with $K = 0$ is equivalent to that of the Discrete Fourier Transform (DFT), and the bank of fence filters achieved with $K = 2$ is similar to that of the Taylor²-Fourier transform, except that their oscillating harmonic estimates are instantaneous (without delay). In addition, the computational complexity of these extended filters is much more lower ($6/\text{Log}_2(N)$ for $N > 64$) than that of the Fast Fourier Transform (FFT), so they are very useful for control applications of power systems.

Contents

List of figures	xi
Acronyms	xiv
Nomenclature	xv
1 Introduction	1
2 Instantaneous Oscillating Phasor Estimates with Taylor^K-Kalman Filters	5
2.1 Introduction	5
2.2 Signal Model	8
2.3 Kalman Filter	10
2.4 Numerical Results	11
2.4.1 Signal Test	11
2.4.2 Magnitude and Phase Step Estimates	22
2.4.3 Frequency Step Estimates	24
2.5 Experimental Results	27
2.6 Discussion	30
2.7 Conclusions	31
3 Frequency Response of Taylor^K-Kalman-Fourier Filter for Instantaneous Oscillating Phasor Estimates	33
3.1 Introduction	33
3.2 Signal Model and Kalman Filter	35
3.3 Taylor-Kalman filter Frequency Response	36
3.3.1 Signal Test	36
3.3.2 Taylor ⁰ -Kalman Filter Frequency Responses	37

3.3.3	Taylor ² -Kalman Filter Frequency Response	39
3.4	Taylor ^K -Kalman-Fourier Filter	40
3.4.1	Taylor ⁰ -Kalman-Fourier Filter	42
3.4.2	Taylor ² -Kalman-Fourier Filter	43
3.5	Numerical Results	44
3.6	Conclusions	47
4	Taylor^K-Kalman-Fourier Differentiators for Instantaneous Derivative Estimates	48
4.1	Introduction	48
4.2	Taylor ^K -Kalman Differentiators	51
4.2.1	Taylor Signal model	51
4.2.2	Differentiator Frequency responses	52
4.2.3	Taylor ² -Kalman Differentiator Frequency response	53
4.3	Low-Pass Taylor ^K -Kalman Differentiator	53
4.4	Taylor ^K -Kalman-Fourier Differentiators	59
4.5	Numerical Results	62
4.5.1	Taylor ^K -Kalman Differentiators	62
4.5.2	Low-Pass Taylor ^K -Kalman Differentiators	63
4.5.3	Taylor ^K -Kalman-Fourier Differentiators	63
4.5.4	Power Swing Signal Decomposed by T ² -K-F Differentiators	65
4.6	Conclusions	66
5	Conclusions	68
5.1	Contributions	69
5.2	Future Work	69

List of figures

- 1.1 Difference between static and dynamic phasor. 2
- 2.1 Signal (amplitude, per unit (pu)) and error estimation with zeroth-order signal model. 12
- 2.2 Amplitude and phase estimation using the zeroth-order signal model. . . . 13
- 2.3 Phasor complex path (– line) and estimate(– · line and point) produced with the zeroth-order signal model. 14
- 2.4 Total vector error achieved with the zeroth-order truncated model. 15
- 2.5 Signal and error estimation obtained with the second-order signal model. It is reduced by a factor of ten. 16
- 2.6 Amplitude and phase estimation with the second-order signal model and the error estimate. 17
- 2.7 Phasor complex path (dots) and estimate(line) obtained with the second-order signal model. 18
- 2.8 Total vector error (TVE) achieved with the second-order truncated model. It is reduced by a factor of ten. 18
- 2.9 Speed and frequency estimates obtained with the second-order signal model. 19
- 2.10 Speed and frequency normalized error obtained with the second-order model. 20
- 2.11 Magnitude of the Kalman gains. 20
- 2.12 Root mean square of the TVE (in %) as a function of sampling frequency ($M = 2^m$ samples per cycle) and degree K of the Taylor polynomial. . . . 22
- 2.13 Magnitude and phase estimates obtained with the zeroth- and second-order Kalman filter for the magnitude and phase step signal. 23
- 2.14 Phasor trajectories of the zeroth- and second-order filters. The spiral corresponds to the estimates obtained with the zeroth-order filter, and lasts twelve fundamental cycles. 24

2.15	Estimates of amplitude and phase first derivatives obtained with the second-order Kalman filter from the amplitude and phase step signal.	25
2.16	Magnitude and phase estimates obtained with the zeroth and second-order Kalman filter from the frequency step test signal.	26
2.17	Phasor trajectories obtained with the zeroth- and second-order filters from the frequency step test signal.	27
2.18	Estimates of amplitude and phase first derivatives obtained with the second-order Kalman filter from the frequency step test signal.	28
2.19	Test signal and signal estimation error.	29
2.20	Estimates of amplitude and phase with $K = 0, 2$ and their first derivatives obtained with the second-order Kalman filter from the test signal.	29
2.21	Improved estimates without the fifth harmonic interference.	30
3.1	Frequency responses of the Taylor ⁰ -Kalman filter.	37
3.2	Magnitude responses of the Kalman filter.	38
3.3	Magnitude responses of the Taylor ⁰ -Kalman-dc filter.	39
3.4	Magnitude responses of the dc filter for different sampling frequencies.	40
3.5	Frequency response of T ² -K filter for several sampling frequencies.	41
3.6	Frequency response to the $T^0 - K - F$ filter.	42
3.7	Frequency response to the $T^2 - K - F$ filter.	44
3.8	Magnitude response of the first and second differentiators (T ² -K-F).	45
3.9	Signal and error estimates.	46
3.10	Phasor and first derivative estimates with $K = 0$ and $K = 2$	47
4.1	Magnitude and phase response of the zeroth T ² -K differentiator. The frequency response is flat around the null frequency.	54
4.2	Magnitude response of the first and second T ² -K differentiators. Note the linear and parabolic gains around the null frequency.	55
4.3	Phase response of the first and second T ² -K differentiators. Close to the zero frequency, they have the ideal phase responses ($j\omega$, and $(j\omega)^2$).	56
4.4	Magnitude and phase response of the zeroth LP T ² -K differentiator.	57
4.5	Magnitude response of the first and second LP T ² -K differentiators.	58
4.6	Phase response of the first and second LP T ² -K differentiators.	58

4.7	Magnitude response of the first three Taylor ^K -Kalman-Fourier differentiators for $K = 2, 3$, and 32 harmonics. Note that ideal differentiator gains are achieved about null frequency and full rejection about harmonic frequencies.	60
4.8	Phase response of the first three Taylor ^K -Kalman-Fourier differentiators for $K = 2, 3$, and 32 harmonics. Close to the zero frequency, they have the ideal phase responses ($j\omega$, and $(j\omega)^2$).	61
4.9	Signal, speed and acceleration estimates obtained with T ² -K differentiators.	62
4.10	Signal, speed and acceleration estimates obtained with T ³ -K differentiators.	63
4.11	Derivative estimates obtained with the LP T ² -K differentiators.	64
4.12	Derivative estimates obtained with the LP T ³ -K differentiators.	64
4.13	Derivative estimates obtained with the T ^K -K-F differentiators for $K = 2, 3$ and including 32 harmonics.	65
4.14	At the top, amplitude (continuous line) and derivative (dash line) instantaneous estimates of a swing current (in dots) in a power system at 50Hz. At the bottom, the instantaneous phase (continuous line) and frequency (dashed line) estimates of the same signal. Those estimates were obtained with the T ² -K-F differentiators.	66

Acronyms

LS	Least Square.
LQ	Linear Quadratic Optimal Control.
PMU	Phasor Measurement Unit.
FFT	Fast Fourier Transform.
WGN	Wight Gaussian Noise.
WLS	Weighted Least Squares.
FIR	Finite Impulse Response.
SNR	Signal Noise Ratio.
TVE	Total Vector Error.
NRMSE	Normalized Root Mean Square.
rms	root mean square.
DFT	Discret Fourier Transform.
WANs	Wide Area Networks.
TFT	Taylor ^K -Fourier Transform.
KF	Kalman Filter.
MISO	Multiple-Input Single-Output.
OFDM	Orthogonal Frequency-Division Multiplexing.
ARMA	Autoregressive Moving Average.
DHT	Digital Hilbert Transformer.
IIR	Infinite Impulse Response.
T^K-K	Taylor ^K -Kalman.
LP T^K-K	Low-Pass Taylor ^K -Kalman.
T^K-K-F	Taylor ^K -Kalman-Fourier.

Nomenclature

Re	Real number.
$!$	Factorial.
j	Imaginary unit.
$-$	Complex conjugate.
T	Transposed.
$\hat{\mathbf{x}}$	\mathbf{x} estimate.
\mathbf{x}^-	\mathbf{x} A priori.
H	Hermitian.
σ_v^2	Variance of input noise.
σ_w^2	Variance of measurement noise.
\mathbf{I}	Identity matrix.
z	z -transform.
$\overline{\mathbf{K}}$	steady-state Kalman gains

Chapter 1

Introduction

The principal objective in estimation theory is to achieve the most precise estimation in shortest time; i.e. the closest to the real value, no matter how complex the conditions can be: signal corrupted by noise, or with abrupt changes, etc. If it is possible to obtain better results under the last conditions, then the method is successful. That is why estimation theory is required in different areas, as communication systems, digital signal processing, control, among many others; and with diverse applications such as measurement, monitoring, filtering, and so on.

One of the well known estimation algorithm is the least squares (LS) method, that was developed by Gauss in 1795, and was inspired by the observation of the comets. He used that method for estimating the trajectory of comets, based in the a posteriori measurements taken by a telescope [1]. The main disadvantage of this method is that it depends on certain number of observations, and its estimates are always delayed. This is a disadvantage when it is desirable no to have any delay at all in the estimates.

Problem statement

In physics and engineering, a phasor, is complex number used to represent a sine wave whose amplitude (A_0), phase (φ_0), and angular frequency (ω) are time-invariant. The traditional method to obtain phasor estimates is the FFT, which is a special case of LS. Its disadvantage is that it needs several samples for having good estimation. In addition, it assumes a static signal model, i.e. it assumes amplitude, phase and frequency constant, so when the signal has perturbations or the electrical system

moves, the phasor estimates become erroneous. A more convenient estimation method must take into account its fluctuations. On the other hand the Kalman filter does not need to have a big number of samples for achieving a good estimation, it only needs a good state transition matrix, i.e. a signal model.

One of the first publications on phasor estimation using Kalman filter is [2], but its state transition matrix was based also on a steady-state sinusoidal model. In [3] a method was proposed for measurement the rate and severity of periodic voltage fluctuations. In [4] the Kalman filter was implemented on a Zoran ZR34161 Vector Signal Processor (VSP), but again with a static signal model, even if it included a dc component to estimate the offset together with the phasor. Other references that used a steady-state sinusoidal signal model are [5]-[8]. And since then Kalman filter disappeared in subsequent publications on phasor estimation and one-cycle Fourier filter prevailed. In this work we show that the problem lies not in the Kalman algorithm, but in the signal model. Kalman filter is an excellent estimator when it works with a good signal model. So, in this sense, this work resuscitates the Kalman filter in the phasor estimation area.

The left side of Fig. 1.1 shows a static phasor, with constant amplitude A_0 and phase φ_0 , marking a fixed point, and on the right side, a phasor following a line with dynamic amplitude $a(t)$ and phase $\varphi(t)$. The second one can better follow the fluctuations of the power system than the first, which is doomed to be constant.

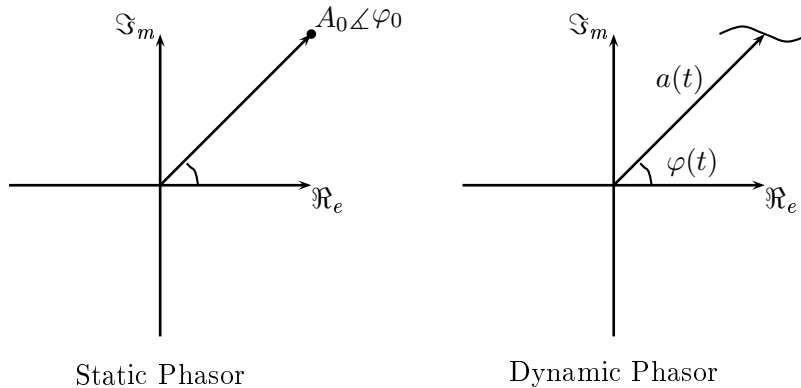


Fig. 1.1: Difference between static and dynamic phasor.

Phasors estimated with such a dynamic signal model, are more flexible and suitable for fluctuating signals, because they can better inherit the movement,

because they are more flexible than the static one. So in this sense, they are truly dynamic in amplitude and phase. With a Taylor polynomial it is possible to approximate the dynamic signal model to the input signal. With this polynomial and its derivatives a state transition matrix for the Kalman algorithm can be established. So, this technique is able to obtain not only better phasor estimates, but also its derivatives. The transient time of these estimates are faster than those of the steady-state signal model used in the traditional Kalman filter, and with the advantage of being instantaneous estimates, for Taylor orders higher or equal to two. Also, for $K = 0$ and when the state transition matrix is extended to include the whole set of harmonic frequencies, it is possible to obtain the FFT, but with less computational cost. Similarly, with $K \geq 2$, the Taylor-Fourier transform can be calculated with less computational cost and with non delayed estimates.

Objective

The principal objective in this work is to develop a methodology for improving the phasor estimates, under smooth oscillations. Other objectives are:

- Study and compare the developed methodology with others methodologies.
- Determine its advantages and disadvantages: in speed, computational load, versatility and exactitude.
- Obtain good results under smooth oscillations or when the signal is corrupted by noise.

The technique leads to a new bank of differentiators with instantaneous derivative estimates for Taylor orders greater or equal to two.

Organization of the thesis

The thesis is organized as follow:

Chapter 2 Develops the Taylor^K-Kalman filter. For Taylor orders greater than zero, this filter reduces the phasor estimation error of the traditional Kalman filter ($K = 0$) under oscillation conditions, abrupt changes and when the signal

is corrupted by white Gaussian noise (WGN), because subspaces with $K \geq 0$ include the zeroth subspace and provide room for oscillatory signals.

Chapter 3 Presents the frequency response of the Taylor^K-Kalman filters, and an extension to the full set of harmonics referred to as the Taylor^K-Kalman-Fourier, reduces sideband gain and provides full rejection around all the included harmonic frequencies. In addition, this filter bank is able to estimate the phasor (the complex envelope) and its derivatives at each harmonic frequency. For $K = 0$ it is equivalent to the DFT, and for $K \neq 0$ is equivalent to the digital Taylor-Fourier transform.

Chapter 4 Deals with the bank of differentiators, focusing our attention to the null frequency, or baseband. This bank is very useful when the interest is placed in estimating the derivatives of a smooth signal (non modulated signal) such as in control applications.

Chapter 5 Summarizes the conclusions of this research work.

Chapter 2

Instantaneous Oscillating Phasor Estimates with Taylor^K-Kalman Filters

2.1 Introduction

Phasor estimation under transient conditions is a hot topic today due to the recent review of the synchrophasor standard [9]. On one hand, the introduction of dynamic conditions to the classical phasor concept broke a very old and fundamental schema very useful in power engineering. On the other, a lack of a unifying theory to explain the behavior and the relationships among the different phasor estimating techniques makes extremely difficult to recommend one.

There are many algorithms for phasor estimation under transient conditions. Even if the standard [9] does not specify a particular phasor estimation method [10], it mentions without referencing them [9, Annex C, Figs: C.1 and C.2] the following three examples: 1 Cycle Rectangular [11], 3 Cycle flat-top [12], and 4 Cycle Raised-Cosine [13]. Attempts to improve the first method under transient conditions and in view of frequency estimation are reported in [14, 15], and [16].

The *dynamic phasor* concept was first proposed in [17] to follow the dynamics of the deviations from the periodic behavior of current and voltages signals in power systems. However, it was defined as the successive estimation of the first Fourier coefficient by a short-time Fourier transform of one cycle, which uses the same static signal model (a signal with constant amplitude, phase and frequency) as the

Fourier filter proposed in [11]. Note that this dynamic qualifier, widely reported in the literature [18], refers more to the inherent recursive nature of the estimation process than to its postulated signal model. It was in [19]-[20] where an estimation improvement was suggested by relaxing amplitude and phase to time functions. Phasors estimated with such a dynamic signal model are therefore more flexible and suitable for fluctuating signals, inheriting their movement flexibility. So in this sense, they are truly dynamic.

The possibility to approach the dynamic phasor with a Taylor polynomial through the least squares method led to the inclusion of Taylor terms to the Fourier transform. This technique, referred to as *Taylor-Fourier transform* [21], uses the weighted least squares (WLS) approximation to find a set of finite impulse response (FIR) filters that provide the best estimates (in the WLS sense) not only of the phasor, but also of its first derivatives, at the middle of the time observation window. One of the main concerns of this technique is the delay of the estimates, due to its time extended signal model.

The main idea of this paper is to use the Kalman filter as an observer able to build (estimate) the input signal with the instantaneous dynamic phasor and its derivatives in a state space vector. It is based on the fact that Kalman filter is a very good signal estimator provided its model fits the input. In our case, the signal estimates depend only on the instantaneous phasor and its complex conjugate. And for the second-order model, the estimates are very good.

Kalman filter was proposed for phasor estimation in protection applications in [22]-[23]. The problem is that its use was intrinsically related to the old static-phasor paradigm (steady-state sinusoidal signal model) as it can be confirmed in [24]-[25]. This also explains why subsequent publications [26]-[27] refer to *the Kalman filter* as if it were only one. In [11], for example, Kalman filter was compared to the half-cycle Fourier filter when the process noise is zero and measurement noise is constant; and since then, the Fourier filter prevailed over the Kalman filter in subsequent publications on phasor estimation. But this comparison did not take into account that the phasor estimates provided by a Fourier signal decomposition are delayed, while those obtained through a Kalman signal decomposition are instantaneous for oscillatory signals. Besides, it is well known that Kalman filter estimates depend fundamentally on its state-space signal model [28], and that its performance is remarkable when it coincides with the input signal.

In this chapter we present the use of the Kalman filter algorithm for finding good observers able to estimate, not only the dynamic phasor, but also its derivatives. The state-space signal model used in the heart of the Kalman algorithm is obtained from the derivatives of the K th-order Taylor polynomial modeling the oscillation envelope. This corresponds to a Taylor approximation to its lowpass signal. The bandpass signal is obtained by a simple modulation operated by a rotation at that fundamental frequency in the complex plane. The main contribution of this chapter is to provide a state-transition matrix with a sinusoidal signal model relaxed by a K th Taylor polynomial to approach the amplitude and phase fluctuations between one signal sample and the next with the Kalman procedure. This flexibility allow the Kalman filter to estimate oscillatory signals with higher accuracy and, at the same time, to provide estimates not only of the instantaneous phasor itself, but also of its derivatives, which are included in the state vector. The estimates obtained in an oscillation example, and the benchmark test signals defined in [9, Appendix G] illustrate the improved performance of this new phasor estimation technique.

The new approach is then very different to the one reported in [15], which estimates the dynamic frequency from two consecutive phasor estimates using a finite-difference equation. In this case errors due to the dynamic conditions propagate to the frequency estimates, which in addition are very sensitive to noise due to the fact that they are based in a finite-difference equation.

The chapter is organized as follows: In section 2.2, the state-space signal model is defined. Then, in Section 2.3, the equations of the Kalman filter as implemented to obtain the results are declared, together with its main reference. Finally, in Sections 2.4, and 2.5 the main results using a zeroth-order and second-order signal model are presented and discussed. The main conclusion of this chapter is that Kalman filter is able to provide, under oscillation conditions, better instantaneous estimates (synchronized and without delay), not only for the phasor itself but also for at least its first derivative. These results are promising and surely will have a positive impact on the conformation of the new synchrophasor norm, because under oscillations these estimates are instantaneous (no delay) while they preserve their synchrony, a crucial attribute for their application.

2.2 Signal Model

In [19, 20] a bandpass signal model was proposed for power system oscillations:

$$s(t) = a(t) \cos(2\pi f_1 t + \varphi(t)) \quad (2.1)$$

in which, $a(t)$ is the amplitude and $\varphi(t)$ the phase of the signal $s(t)$. Bandpass signals are assumed to be narrowband around the central frequency f_1 . This means that amplitude and phase variations are slow with respect to the cyclic wave.

In terms of the complex exponential function the signal model can be simplified as

$$\begin{aligned} s(t) &= \frac{1}{2} (p(t)e^{j2\pi f_1 t} + \bar{p}(t)e^{-j2\pi f_1 t}) \\ &= \operatorname{Re}\{p(t)e^{j2\pi f_1 t}\}, \quad -\frac{T}{2} \leq t \leq \frac{T}{2} \end{aligned} \quad (2.2)$$

in which $p(t) = a(t)e^{j\varphi(t)}$ is referred to as *dynamic phasor*.

The complex dynamic phasor function $p(t)$, can be approximated by a K th Taylor polynomial centered at t_0 :

$$\begin{aligned} p_K(t) &= p(t_0) + \dot{p}(t_0)(t - t_0) + \cdots + p^{(K)}(t_0) \frac{(t - t_0)^K}{K!}, \\ & \quad t_0 - \frac{T}{2} \leq t \leq t_0 + \frac{T}{2}. \end{aligned} \quad (2.3)$$

A state transition matrix can be easily obtained from the derivatives of each Taylor truncated dynamic phasor. For $\tau = t - t_0$ we have:

$$\begin{aligned} p_K(t) &= p(t_0) + \dot{p}(t_0)\tau + \ddot{p}(t_0)\frac{\tau^2}{2!} + \cdots + p^{(K)}(t_0)\frac{\tau^K}{K!} \\ \dot{p}_K(t) &= \dot{p}(t_0) + \ddot{p}(t_0)\tau + \cdots + p^{(K)}(t_0)\frac{\tau^{K-1}}{(K-1)!} \\ & \quad \vdots \quad \quad \quad \vdots \\ p_K^{(K)}(t) &= p^{(K)}(t_0) \end{aligned} \quad (2.4)$$

Finally, the state transition will be given by:

$$\mathbf{p}_K(t) = \mathbf{\Phi}_K(\tau)\mathbf{p}_K(t_0). \quad (2.5)$$

where $\mathbf{p}_K(t)$ is the state vector, and the state transition matrix is of the form:

$$\Phi_K(\tau) = \begin{pmatrix} 1 & \tau & \frac{\tau^2}{2!} & \cdots & \frac{\tau^K}{K!} \\ & 1 & \tau & \cdots & \frac{\tau^{K-1}}{(K-1)!} \\ & & 1 & \cdots & \frac{\tau^{K-2}}{(K-2)!} \\ & & & \ddots & \vdots \\ & & & & 1 \end{pmatrix} \quad (2.6)$$

For a given polynomial order, this approximation is all the more exact as $t \rightarrow t_0$ if $p(t)$ is a smooth function. The truncated model can then be applied at any time instance t_0 with sufficient precision provided that the size of the time interval τ be short. This condition is accomplished between any two digital signal samples because samplers usually apply very short sampling periods with respect to the fundamental period $T_1 = \frac{1}{f_1}$. We assume that the signal is sampled at $N_1 = 64$ samples per cycle, so $\tau = T_1/64$. This is a very short period of time with respect to the slow fluctuations of $p(t)$.

The truncated signal model is given by:

$$s_K(t) = \text{Re}\{\mathbf{h}^T \mathbf{p}_K(t) e^{j2\pi f_1 t}\} = \text{Re}\{\mathbf{h}^T \mathbf{r}_K(t)\} \quad (2.7)$$

where $\mathbf{r}(t)$ is the rotated vector in the time t , and \mathbf{h}^T extracts its first component, i. e. $\mathbf{h}^T = [1 \ 0 \ \cdots \ 0]$, with K zeros.

In terms of the rotated vector, Eq. (2.5) becomes

$$\mathbf{r}_K(t) = \Phi_K(\tau) e^{j2\pi f_1 \tau} \mathbf{r}_K(t_0). \quad (2.8)$$

Assuming $t_0 = (n-1)T_s$ and $t = nT_s$, where T_s is the sampling period ($T_s = 1/N_1 f_1$), we have the following state transition between the discrete rotated vectors:

$$\mathbf{r}_K(n) = \Phi_K(\tau) \psi_1 \mathbf{r}_K(n-1) \quad (2.9)$$

where ψ_1 is the phase factor $\psi_1 = e^{j\theta_1}$, corresponding to the fundamental radian frequency ($\theta_1 = 2\pi f_1 T_s = 2\pi/N_1$). Finally, by defining the state transition equation as

$$\begin{pmatrix} \mathbf{r}_K(n) \\ \bar{\mathbf{r}}_K(n) \end{pmatrix} = \begin{pmatrix} \psi_1 \Phi_K(T_s) & \mathbf{0} \\ \mathbf{0} & \bar{\psi}_1 \Phi_K(T_s) \end{pmatrix} \begin{pmatrix} \mathbf{r}_K(n-1) \\ \bar{\mathbf{r}}_K(n-1) \end{pmatrix}, \quad (2.10)$$

the truncated signal model is given by:

$$s_K(n) = \frac{1}{2} \begin{pmatrix} \mathbf{h}^T & \mathbf{h}^T \end{pmatrix} \begin{pmatrix} \mathbf{r}_K(n) \\ \bar{\mathbf{r}}_K(n) \end{pmatrix}. \quad (2.11)$$

This equation shows the instantaneous dependence of the signal model on the dynamic phasor. The Taylor-Kalman filter is a signal follower that operates as an instantaneous signal decomposer. Its best dynamic rotor estimates will be provided when it reaches its smallest signal estimation error, and this in turn happens when the input signal is in the subspace spanned by the signal model. This is precisely the case of smooth oscillations in a second order subspace ($K = 2$), as we will see in the numerical results, in which signal estimation errors of millionths are reached.

The state transition matrix in (2.10) is complex $2(K + 1) \times 2(K + 1)$ and works with the rotated phasors, so to get the dynamic phasor estimates with the Kalman filter they must be anti-rotated to eliminate the its factor. Note that the state space model in (2.10) contains genetic information of the development of the complex trajectory from one sample to the next. The steady-state signal model ($K = 0$) would oblige the phasor to move in circles from one sample to the next. With the Taylor state transition matrix in (2.6), the phasor estimates are allowed to move in more flexible trajectories, bounded by the highest order term in the polynomial.

In the next section, we consider how these truncated signal models are used in the Kalman filter. This filter decompose the input signal into the state-vector components. The Kalman decomposition and its estimates are instantaneous under oscillatory conditions, without the delay of the Fourier filter decomposition.

2.3 Kalman Filter

In this section the development of the Kalman filter in [29, pp. 381-384] is followed. Other references can be found in [30, 28, 11]. The state vector model is

$$\mathbf{x}(n) = \mathbf{\Phi}\mathbf{x}(n - 1) + \mathbf{\Gamma}v(n), \quad (2.12)$$

in which the state transition matrix is the one in (2.10) and $\mathbf{\Gamma}^T = (\mathbf{h}^T \ \mathbf{h}^T)$ since white Gaussian noise (WGN) $v(n)$ is assumed to affect only rotated phasor component, i.e., the derivatives are not affected by noise.

On the other hand, the observation (or measurement) model is

$$s(n) = \mathbf{H}\mathbf{x}(n) + w(n) \quad (2.13)$$

We also assume the signal is affected by additive WGN through $w(n)$. Finally for both models we have $\mathbf{H} = (\mathbf{h}^T \ \mathbf{h}^T)$.

The Kalman recursive process will be defined by the following sequence for the n th cycle:

1. Time update:

(a) State prediction

$$\hat{\mathbf{x}}^-(n) = \mathbf{\Phi}\hat{\mathbf{x}}(n-1) \quad (2.14)$$

(b) *A priori* error covariance

$$\mathbf{P}^-(n) = \mathbf{\Phi}\mathbf{P}(n-1)\mathbf{\Phi}^H + \mathbf{\Gamma}\mathbf{\Gamma}^T\sigma_v^2 \quad (2.15)$$

2. Measurement update

(a) Kalman gain:

$$\mathbf{K}(n) = \mathbf{P}^-(n)\mathbf{H}^T(\mathbf{H}\mathbf{P}^-(n)\mathbf{H}^T + \sigma_w^2)^{-1} \quad (2.16)$$

(b) State update

$$\hat{\mathbf{x}}(n) = \hat{\mathbf{x}}^-(n) + \mathbf{K}(n)(s(n) - \mathbf{H}\hat{\mathbf{x}}^-(n)) \quad (2.17)$$

(c) *A posteriori* error covariance

$$\mathbf{P}(n) = (\mathbf{I} - \mathbf{K}(n)\mathbf{H})\mathbf{P}^-(n) \quad (2.18)$$

Where σ_v^2 and σ_w^2 are the variances of the input and measurement noise respectively. The process starts with $\mathbf{x}(0) = \mathbf{0}$, and $\mathbf{P}(0) = 10^9\mathbf{I}$ for the initial unknown state error covariance matrix. Note that once the optimal Kalman gains are established, the computational burden of the filtering process is reduced only to Eqs. (2.14), (2.17), and the anti-rotation.

2.4 Numerical Results

2.4.1 Signal Test

The signal in (2.1) with the following amplitude and phase time functions will be taken as signal test:

$$a(t) = a_0 + a_1 \sin(2\pi f_a t) \quad (2.19)$$

$$\varphi(t) = \varphi_0 + \varphi_1 \sin(2\pi f_\varphi t) \quad (2.20)$$

with the following parameters in amplitude: $a_0 = 1$, $a_1 = 0.1$, and $f_a = 5\text{Hz}$, and phase: $\varphi_0 = 1$, $\varphi_1 = 0.1$, $f_\varphi = 5\text{Hz}$. And $\sigma_v^2 = 0.01$ and $\sigma_w^2 = 10^{-4}$ which corresponds to a signal to noise ratio (SNR) of 37 dB, equivalent to the one produced by analog to digital converter of 6 bits. In addition to white noise, the algorithms were tested with pink noise [31] and basically the same error thresholds and behavior were found. It is worth mentioning that the IEEE standard of synchrophasors for power systems [9] does not contain any specification concerning the analog to digital conversion of the input signal in the phasor measurement unit [10] and less still any reference to different types of noise.

Zeroth-order Model

The following are the results obtained with the zeroth-order truncation model Φ_0 which correspond to a zeroth-order Taylor polynomial.

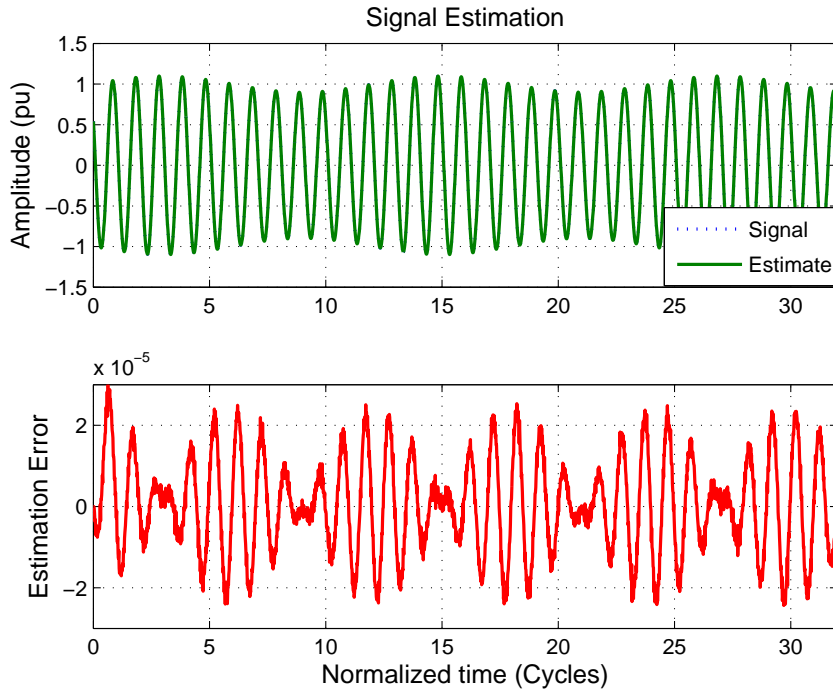


Figure 2.1: Signal (amplitude, per unit (pu)) and error estimation with zeroth-order signal model.

As can be seen in Fig. 2.1, the Kalman filter with the zeroth-order state transition matrix provides good signal estimates. It achieves signal estimation errors

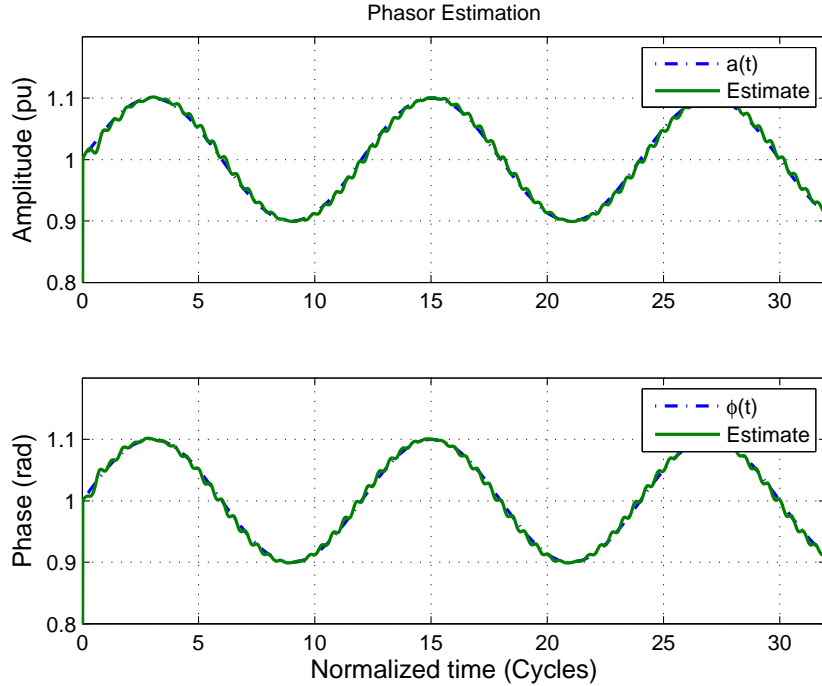


Figure 2.2: Amplitude and phase estimation using the zeroth-order signal model.

in the order of magnitude of 10^{-5} . Unfortunately our problem is not to estimate the input signal but the phasor. The ideal amplitude and phase components of the phasor are shown in Fig. 2.2 in lines and point, while their estimates in continuous lines. Note that a lag and a lead, of about a quarter of a cycle, are perceptible in the amplitude and phase estimates, indicating the presence of a group delay in the transfer function of the filter. The estimates exhibit an undesirable corrugated behavior similar to the infiltrations on the celebrated one-cycle Fourier filter (see Fig. 5 in [13]). This behavior can be perceived with more clarity in the complex path followed by the estimates as shown in Fig. 2.3. The Kalman gains are real and converge to 0.9902 after the first three fundamental cycles. Fig. 2.4 illustrates the behavior of the total vector error (TVE), which is similar to the one in Fig. 10 in [13]. As we can see, even if the Kalman filter provides good signal estimates with the zero-th order model, its phasor estimates are not as good as desired because its undesirable corrugation. In addition, with the zeroth-order model it is impossible to estimate the speed or the acceleration of the phasor. In the next subsection the improvement of the estimates obtained with the Kalman filter using the second-order signal model is shown.

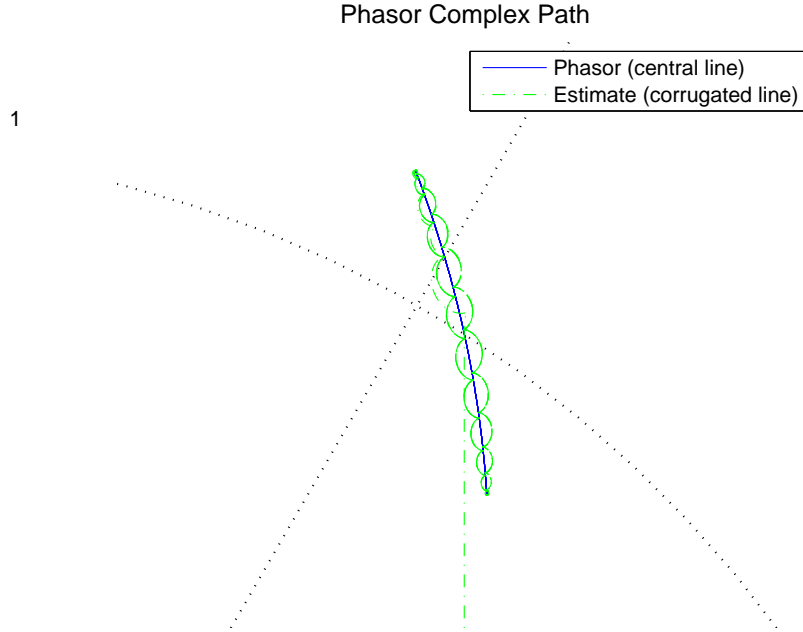


Figure 2.3: Phasor complex path (— line) and estimate(— · line and point) produced with the zeroth-order signal model.

Second-order Model

Once the optimal Kalman gains are established it is possible to use the Kalman filter as an observer with the following Eqs:

$$\hat{\mathbf{x}}^-(n) = \mathbf{\Phi}\hat{\mathbf{x}}(n-1)$$

and

$$\hat{\mathbf{x}}(n) = \hat{\mathbf{x}}^-(n) + \mathbf{K}(n)(s(n) - \mathbf{H}\hat{\mathbf{x}}^-(n)).$$

The following results are obtained with the second-order model ($\mathbf{\Phi}_2$), for which the state transition matrix is 6×6 . We apply the same noise levels of the previous case, $\sigma_v^2 = 0.01$ and $\sigma_w^2 = 10^{-4}$, and the same starting matrix covariance matrix $\mathbf{P}(0)$.

It can be seen in Fig. 2.5 that the signal estimates are improved. With this model, the order of magnitude of the signal estimation error is reduced by one. The increase in model order improves also the phasor estimates, which are now closer to the ideal amplitude and phase sequences as can be seen in Fig. 2.6. It is apparent that the corrugate effect on the previous estimates has disappeared. The lead-lag

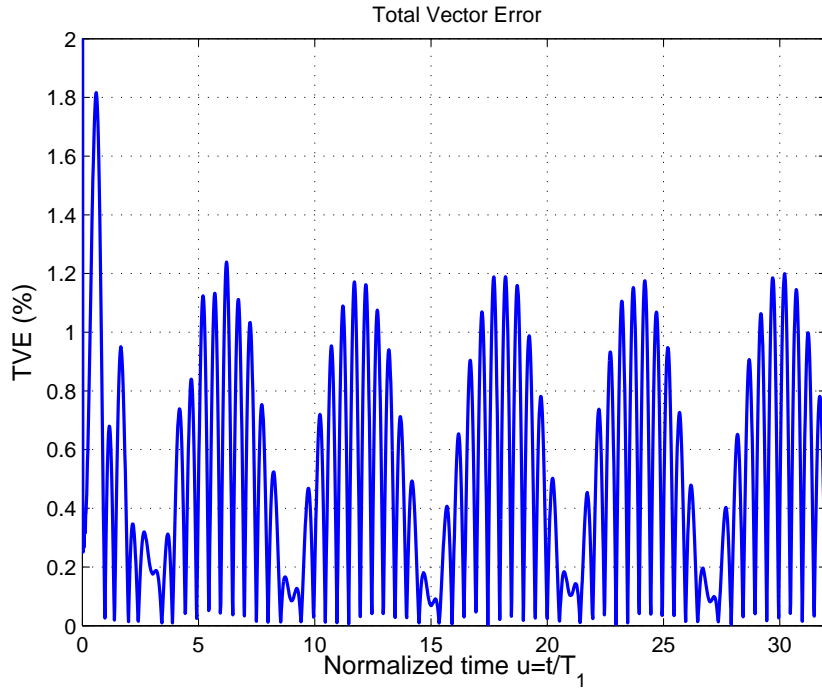


Figure 2.4: Total vector error achieved with the zeroth-order truncated model.

of the previous estimates have also disappeared, indicating that the phase response of this filter is zero flat about the fundamental frequency. So, in this case, the estimates have no amplitude or phase distortion, and therefore are instantaneous. The fluctuation around 0 cycle are due to the adaptive process of the Kalman filter, which starts with free gains at the origin, but they are frozen when they arrive to their first steady-state. The disappearance of the corrugation effect can be confirmed in Fig. 2.7, which illustrates a smoother complex path closer to the ideal one given by the dots. Finally, Fig. 2.8, shows the behavior of the TVE, which is reduced by a factor of ten with respect to the previous case.

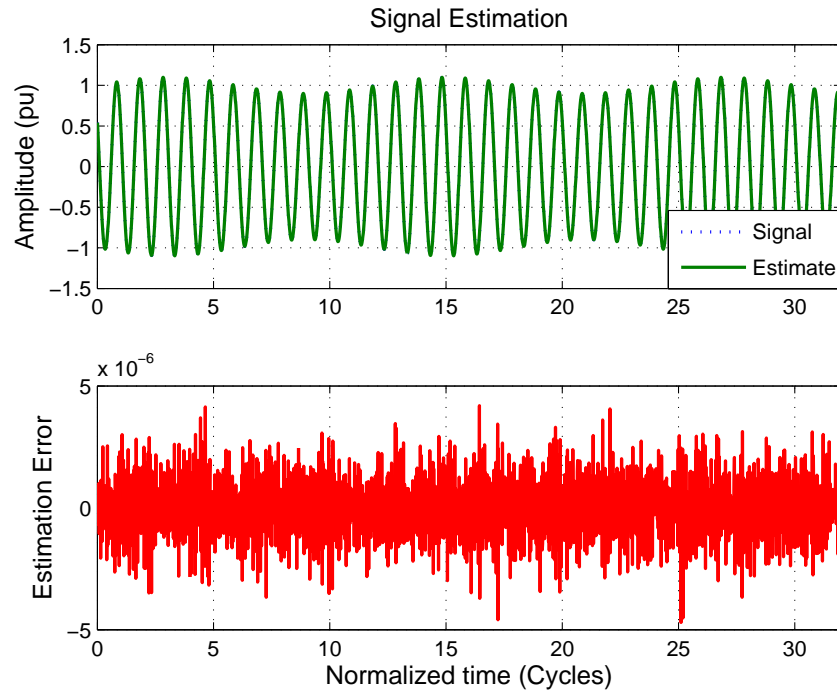


Figure 2.5: Signal and error estimation obtained with the second-order signal model. It is reduced by a factor of ten.

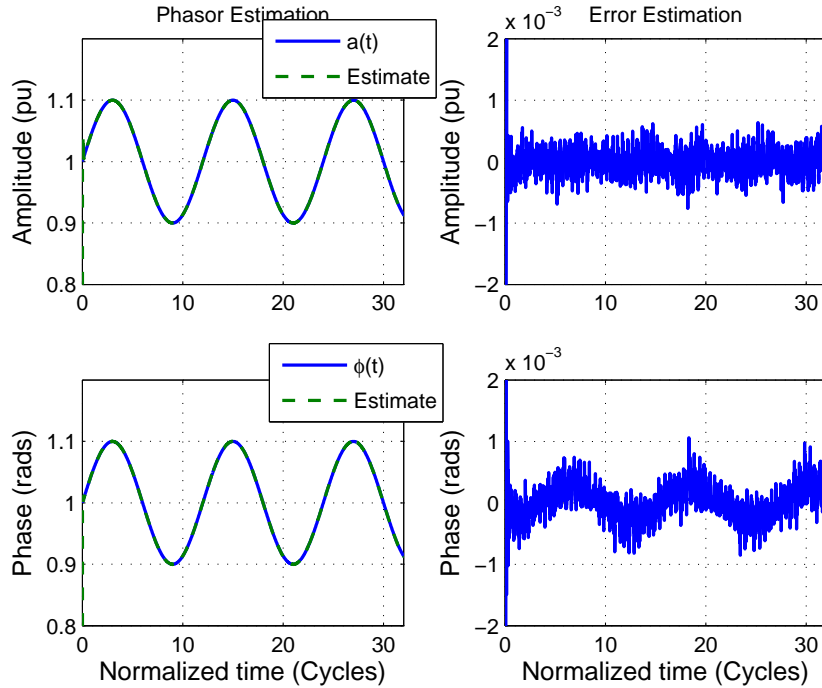


Figure 2.6: Amplitude and phase estimation with the second-order signal model and the error estimate.

With the second-order model it is possible to obtain estimates of the first phasor derivative as it can be seen in Fig. 2.9, in which the first derivative of amplitude and phase are shown (solid lines) with their estimates (dashed lines). These derivatives correspond to the amplitude speed of the oscillation and to the frequency offset (with respect to the fundamental frequency) respectively. It is apparent that these estimates are not as smooth as the phasor estimates, due to their apparent wavering behavior. However, these results are better than those shown in [28, Chapter 5, Fig. 5.17]. The wavering effect is most evident in Fig. 2.10, which illustrates the error of the estimates normalized by the peak values. Due to the fact that phasor derivatives cross through zero, TVE cannot be applied. Instead, the normalized *rms* error (NRMSE) of speed and frequency offset are calculated, and equal to 0.0332 and 0.0560, respectively.

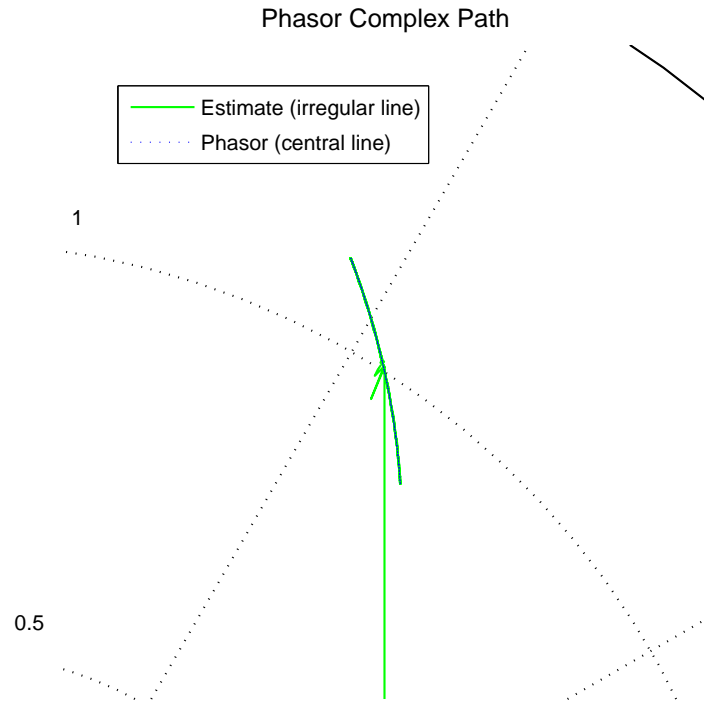


Figure 2.7: Phasor complex path (dots) and estimate(line) obtained with the second-order signal model.

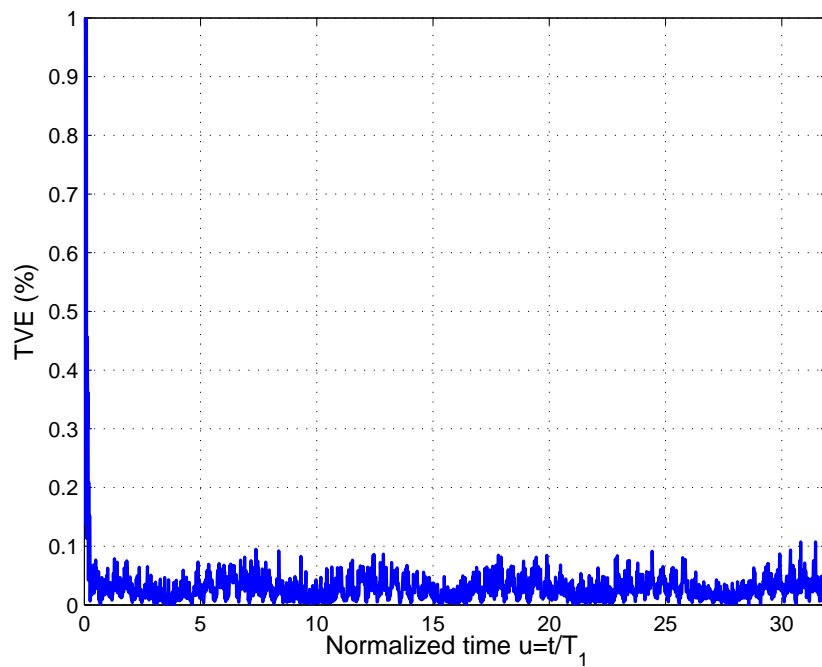


Figure 2.8: Total vector error (TVE) achieved with the second-order truncated model. It is reduced by a factor of ten.

Signal estimation error is reduced ten times more with the fourth-order model, however a slighter reduction in TVE and NRMSE error level is achieved by further increasing the order of the signal model.

The Kalman gain vector of this example was taken from its first steady-state period occurring at the end of the first fundamental cycle. It was observed that in the first five fundamental cycles, the estimates behave like those shown in the previous figures, but after that interval of time degraded to a behavior very similar to that of the zeroth-order model. So the Kalman gain vector of the first steady-state period, as it can be seen in Fig. 2.11 was frozen in the observer whose results were shown. The vector gain for the first half of the state vector is the following: $\mathbf{K} = (0.99208 - 1.6051i, 167.21 - 406.19i, 8538.9 - 4,4603.0i)^T$. The second half is the complex conjugate of the first one.

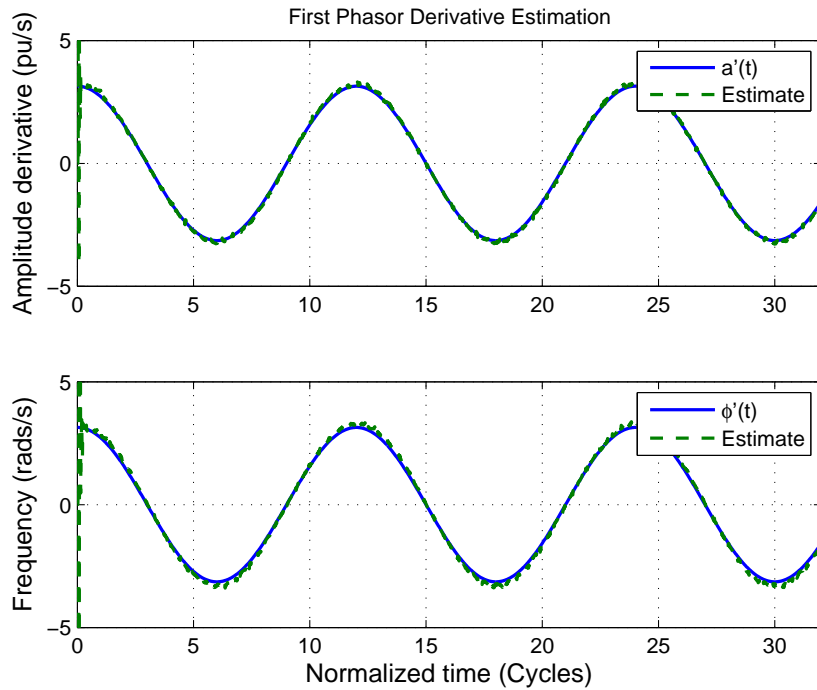


Figure 2.9: Speed and frequency estimates obtained with the second-order signal model.

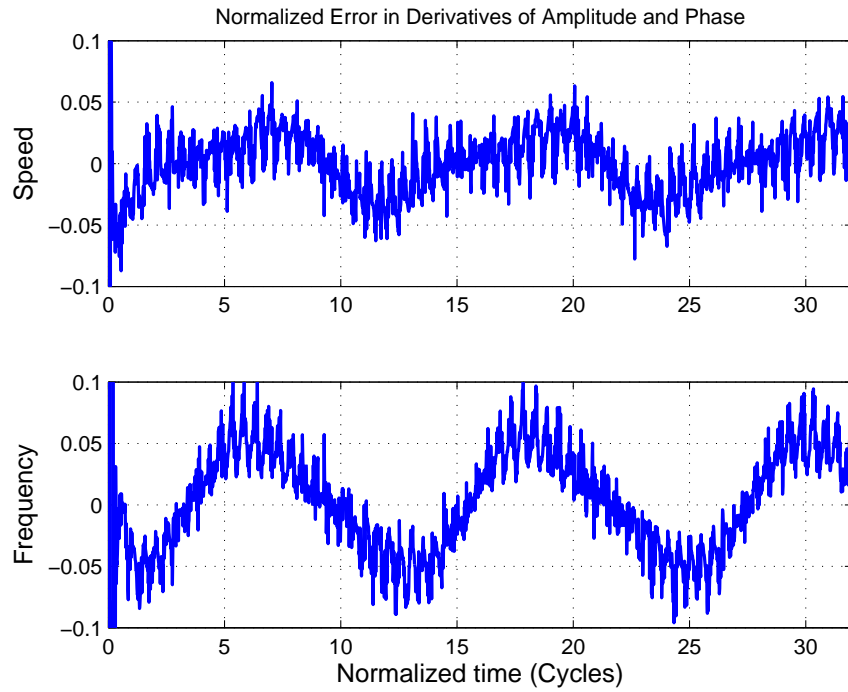


Figure 2.10: Speed and frequency normalized error obtained with the second-order model.

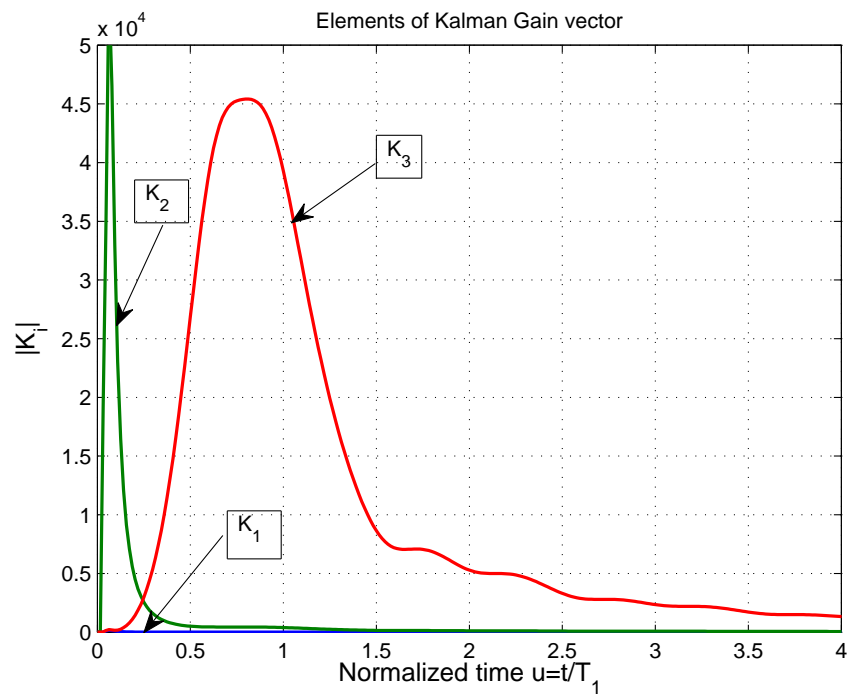


Figure 2.11: Magnitude of the Kalman gains.

TVE Reduction

It is interesting to analyze the behavior of TVE when the sampling frequency or the order of the Taylor polynomial used in the signal model change. Fig. 2.12 shows the *root mean square* of the TVE in percent as a function of those parameters. The *rms* is defined as:

$$rms(TVE) = \sqrt{\frac{1}{N} \sum_{n=1}^N TVE_n^2} \quad (2.21)$$

over the samples in an integer number of oscillation cycles. This is a good measure of the mean error level (given in %). As can be seen in that figure, the error levels with $K = 0$ are almost equal to those with $K = 1$; and also for $K = 2, 3$ and 4. This behavior indicates that the quadratic Taylor element in the signal model is crucial for reducing the error of the phasor estimates. These results indicate that the high estimation errors of the filters for $K = 0, 1$ are mainly due to their phase distortion (delay). These filters are unable to form a flat-null phase gain at the fundamental frequency, in contrast to those for $K \geq 2$. This inability to form a flat-null gain is also a shortcoming of the Fourier filter which has a constant delay. As the sampling frequency increases, a finer continuous shape emerge in the waveforms of the TVE error, as those illustrated in Figs. 2.4 or 2.8. The slow error level augmentation at the higher sampling frequencies in the second curve can be explained by a slight increase in sensitivity to noise at those high frequencies. On the other hand, it was also observed that the estimates of the derivatives are improved when the order of the Taylor polynomial is increased. In the $K = 0, 1$ cases, Kalman gains converge quickly to constant values, however in the $K = 2, 3$, and 4, the gains have a steady-state period, like the one illustrated in Fig. 2.11. All those Kalman observers used the gains achieved at the center of those steady-state periods, determined by a different sample index, depending on the sampling frequency, but almost the same for each of the three different orders.

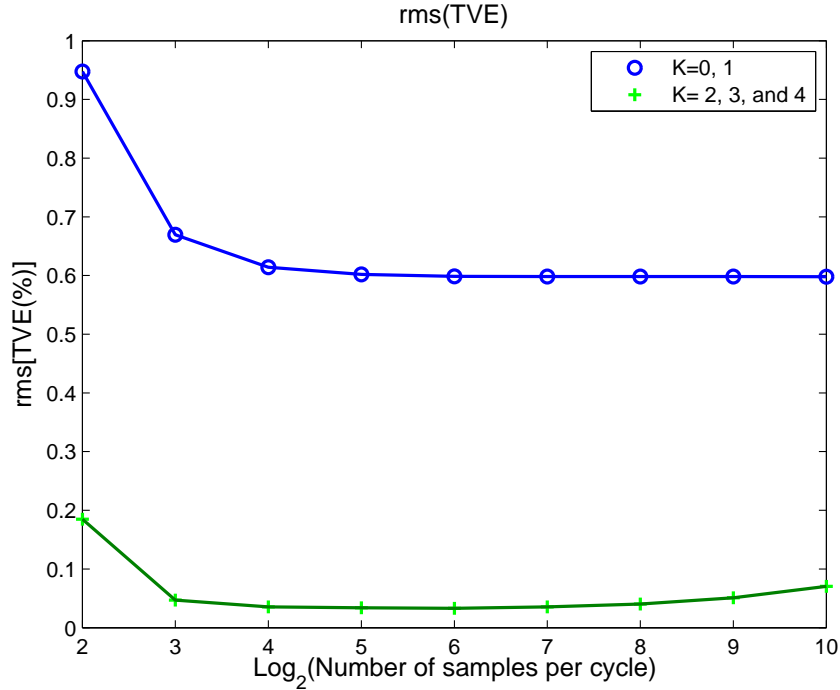


Figure 2.12: Root mean square of the TVE (in %) as a function of sampling frequency ($M = 2^m$ samples per cycle) and degree K of the Taylor polynomial.

2.4.2 Magnitude and Phase Step Estimates

To illustrate the transient response of the filters, both magnitude and phase steps of the benchmark tests in [9, Annexes G.2 and G.3] were mixed together in the analyzed signal. Fig. 2.13 illustrates amplitude and phase transients of the phasor estimates obtained with the zeroth- and second-order Kalman filters from the tested signal. These correspond to the step response of the Kalman filters and are formed by the dominant poles of the corresponding transfer functions. The zeroth-order filter produces long amplitude and phase swings, which correspond to a spiral trajectory in the complex plane centered at the final phasor value, as it can be seen in Fig. 2.14. This transient lasts around twelve cycles, indicating the presence of resonant poles close to the unit circle in the z plane. The second-order filter transient is much lower and shorter (around two-cycles long) than the preceding one. Finally, the estimates of the phasor first derivative provided by the second-order filter are illustrated in Fig. 2.15. It is apparent that the magnitude and phase derivative transient responses last again around two cycles with large estimated values close to the origin, as it was expected from the derivative of a step changes. This high value

is due to the amplitude and phase discontinuities at zero of the test signal, in which the Taylor model is not as appropriate as in the former case of smooth amplitude and phase fluctuations.

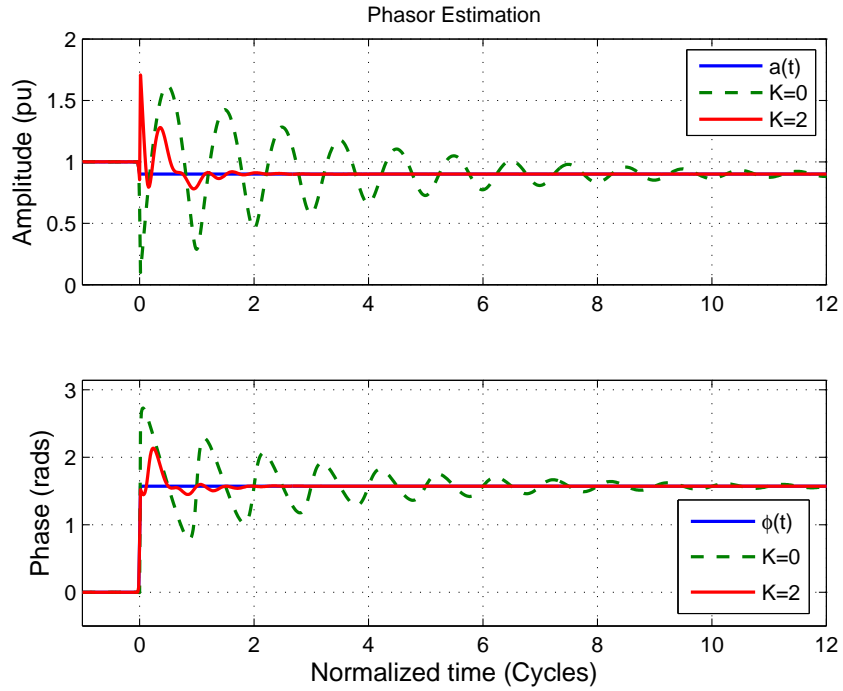


Figure 2.13: Magnitude and phase estimates obtained with the zeroth- and second-order Kalman filter for the magnitude and phase step signal.

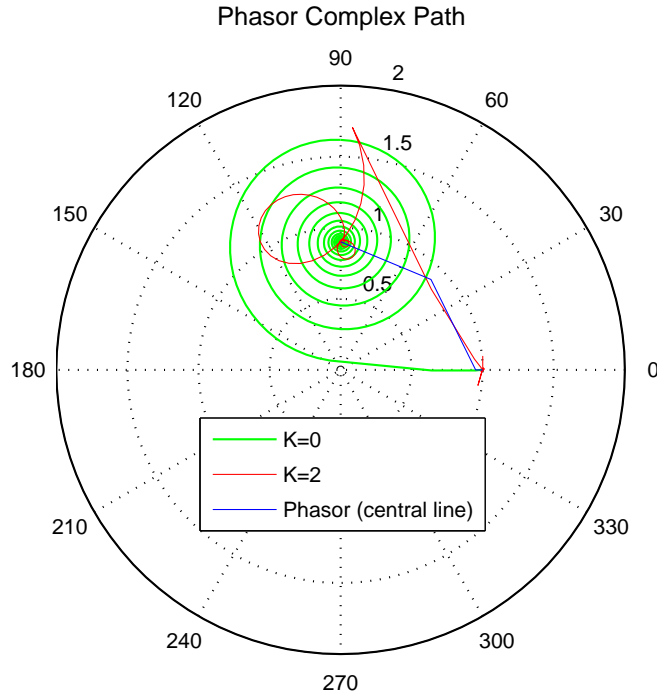


Figure 2.14: Phasor trajectories of the zeroth- and second-order filters. The spiral corresponds to the estimates obtained with the zeroth-order filter, and lasts twelve fundamental cycles.

2.4.3 Frequency Step Estimates

Finally, the estimates of the frequency step test (+5 Hz) in [9, Annex G.4] are shown. Fig. 2.16 shows the magnitude and phase estimates obtained with the compared filters. Note that both filters have comparable performance in the phase estimates but not in the magnitude estimates. This discrepancy is better understood in Fig. 2.17 which shows the phasor trajectory of the estimates in the complex plane. The zeroth-order filter produces considerable magnitude error due to its cycloid behavior in the complex plane. Finally, Fig. 2.18 shows the phasor derivative estimates obtained with the second-order filter. Note that the frequency estimates converge to the ideal frequency step after two cycles. A perceptible error is inevitable due to the fact that the frequency step signal moves away from the frequency of the rotation imposed to the signal model. The small swings after the second cycle are certainly due to the infiltration of the negative fundamental component because that

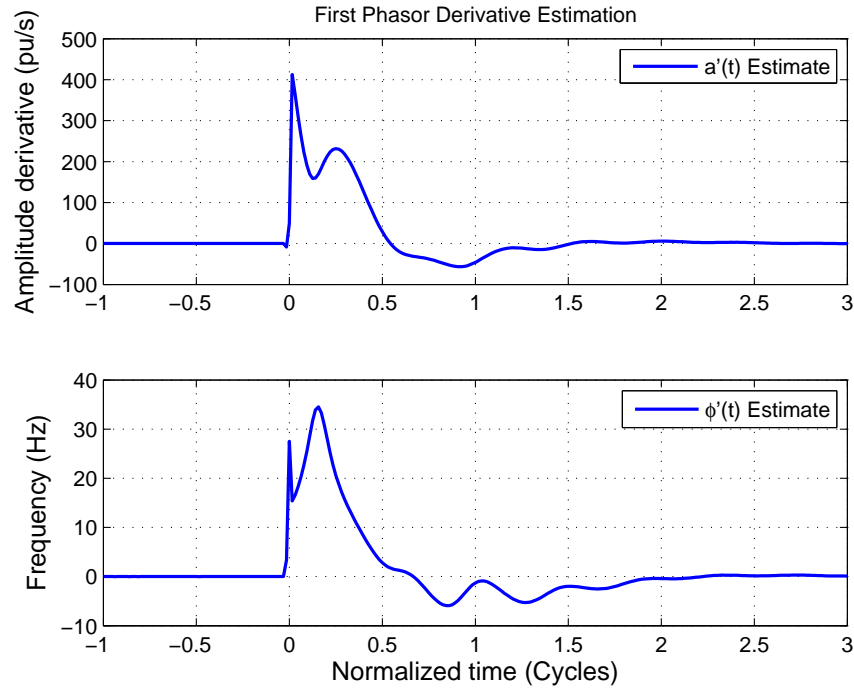


Figure 2.15: Estimates of amplitude and phase first derivatives obtained with the second-order Kalman filter from the amplitude and phase step signal.

component is seen from 65Hz at -130Hz . The gain around the negative frequency is not zero flat for $K = 0$, and almost zero flat for $K = 2$, but in both cases the error is perceptible. The period of such an infiltration would be of $130/60 = 2.1667$ cycles per fundamental period, which precisely corresponds to the period of the error wave perceived in Figs. 2.16 and 2.18. However, more research must be done for improving the response of the derivative estimates before sharp transients.

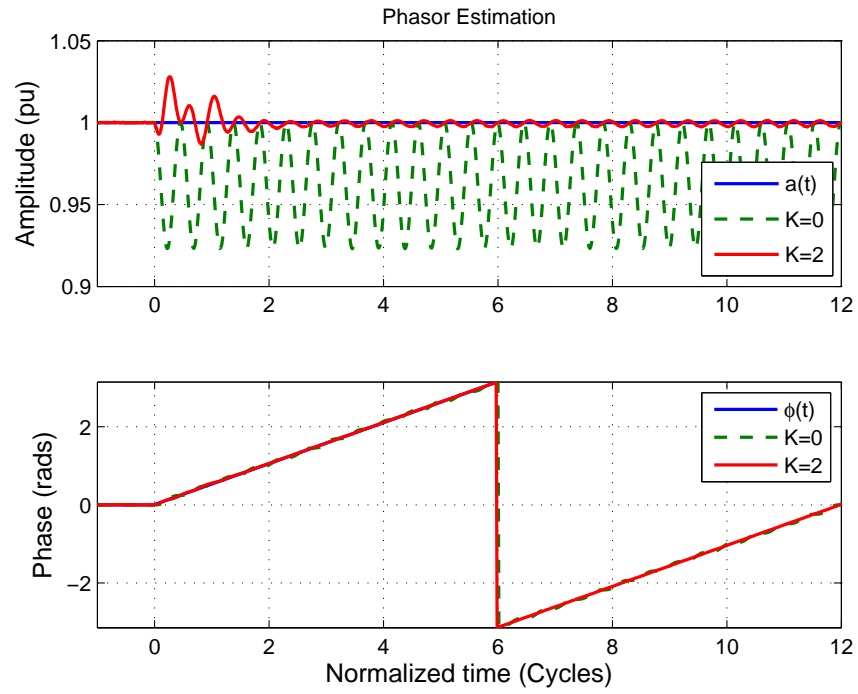


Figure 2.16: Magnitude and phase estimates obtained with the zeroth and second-order Kalman filter from the frequency step test signal.

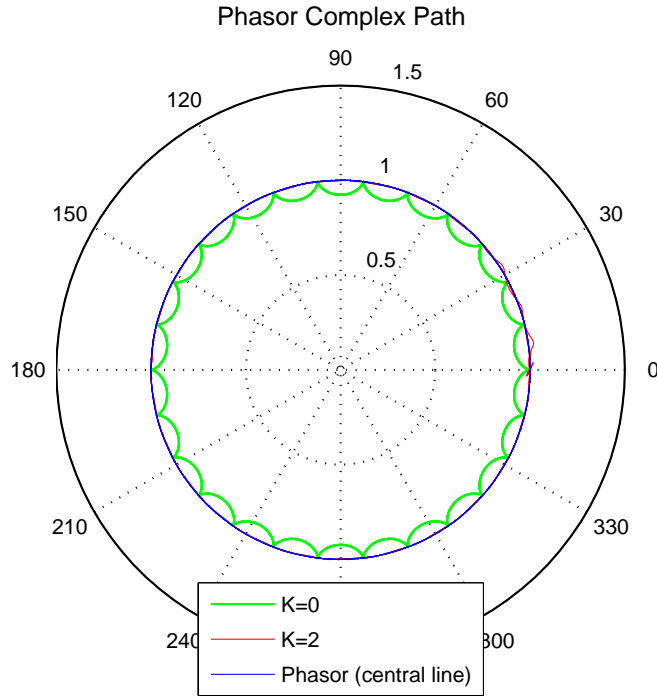


Figure 2.17: Phasor trajectories obtained with the zeroth- and second-order filters from the frequency step test signal.

2.5 Experimental Results

The model used in this paper is based on a band-pass signal. In reality, power system signals may be polluted by harmonics or dc offset which are not covered by this model (see Eqs. (2.10) and (2.11)). In this section the proposed method is applied to a practical signal taken with a PMU from one substation. Fig. 2.19 illustrates the signal as well as the level of estimation error achieved with the zeroth- and second-order estimator. This signal was sampled at 48 samples per cycle. Because it is a signal taken from one substation no further noise was added. Note that the signal estimation error is extremely low, confirming that Kalman filter is a very good signal estimator. The phasor (amplitude and phase) estimates as well as their derivatives are shown in Fig. 2.20. It is apparent that the estimates are noisy. This is due to the presence of a fifth harmonic that infiltrates the estimates according to a spectral analysis applied to the signal. One solution to this shortcoming would be prefiltering

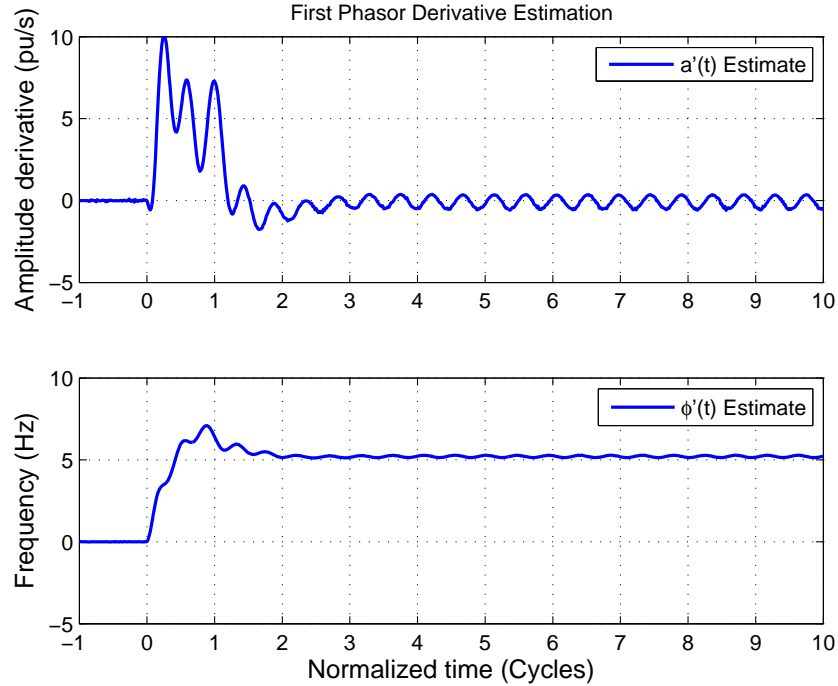


Figure 2.18: Estimates of amplitude and phase first derivatives obtained with the second-order Kalman filter from the frequency step test signal.

the signal with a bandpass filter, but this costs a delay of one or two cycles, plus the additional computation of a convolution per sample. The best solution consists in extending the state transition matrix in (2.10) by including in its diagonal a matrix $\psi_1^h \Phi$ and its complex conjugate per harmonic h , where h is the index of the desired harmonic. This option is more appropriate because it only increases the quantity of Kalman gains by a factor equal to twice the amount of harmonics we want to exclude. Fig. 2.21 shows the estimates obtained through this solution. The improvement in the estimates is apparent, and this implementation needs only double the Kalman gains. we can see that the estimates are very good (the average error in amplitude was reduced from $0.7748 + 0.3897i$ to $0.7735 + 0.3885i$). This extended method allows us to estimate the Taylor-Fourier coefficients [20] or the Fourier coefficients (DFT) with the Kalman filter. The number of products per state estimate is $(2H + 1)[(K + 1)^2 + 2(K + 1)]$ when the signal model contains H harmonics and the dc component.

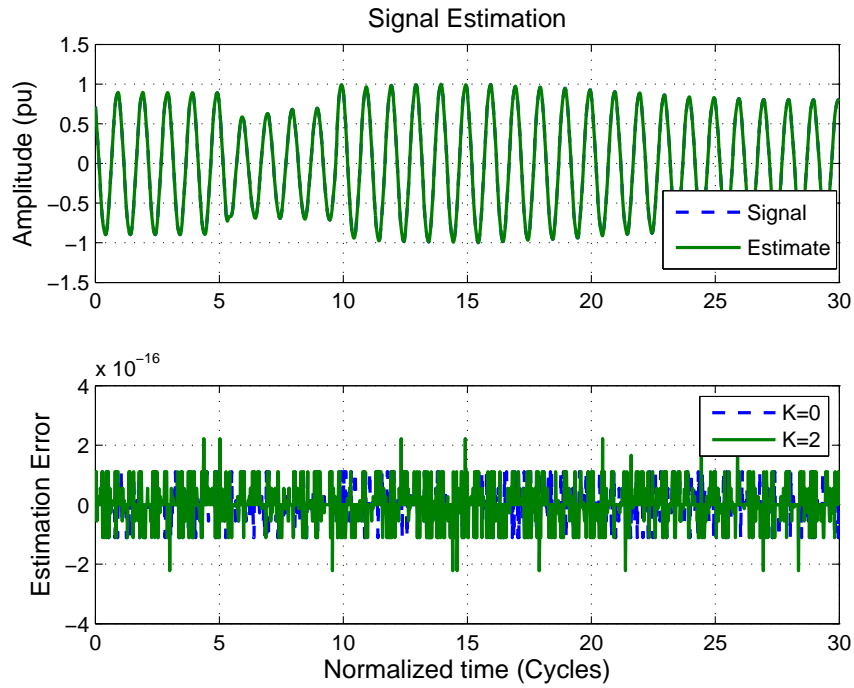


Figure 2.19: Test signal and signal estimation error.

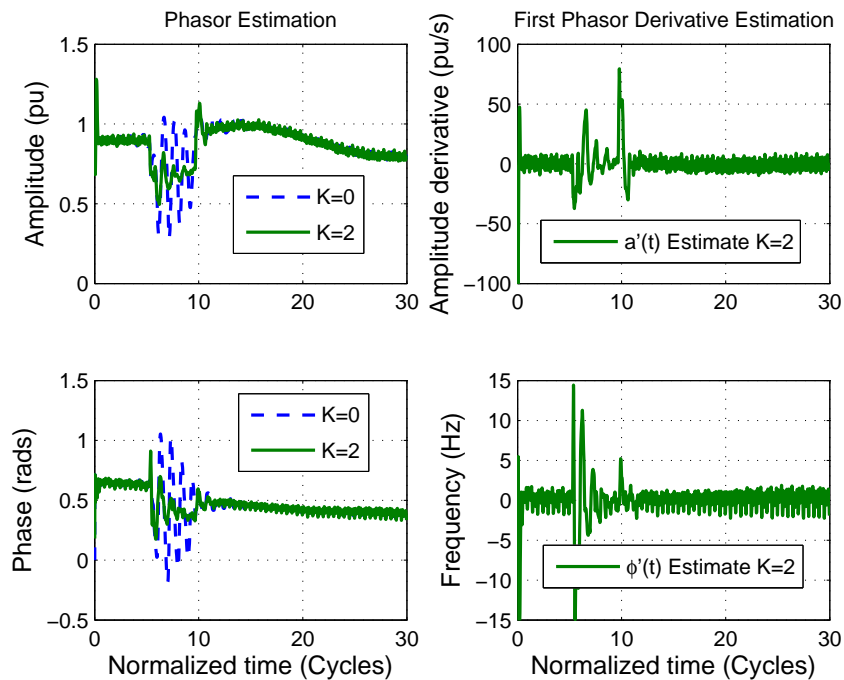


Figure 2.20: Estimates of amplitude and phase with $K = 0, 2$ and their first derivatives obtained with the second-order Kalman filter from the test signal.

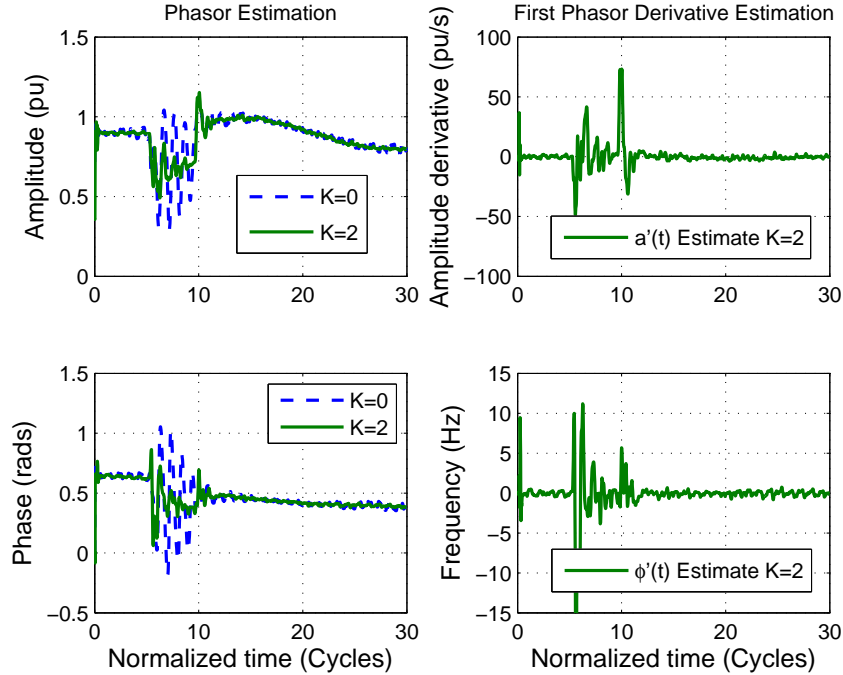


Figure 2.21: Improved estimates without the fifth harmonic interference.

2.6 Discussion

The interest of phasor estimation, in the computer relaying context, is much more placed on signals with abrupt changes than on signals under oscillations. This emphasis explains why the one-cycle Fourier filter is the prototype of this particular application, because in a sudden change it reaches good estimates from one static state to the following one. It also explains that the synchrophasor standard [9], is up to now based on a static phasor model, in a clear contradiction with the dynamic nature of oscillations. And even when it is applied recursively, its estimates inherit that strong static condition.

The dynamic phasor is not dynamic because it is applied recursively, but because provided with a dynamic signal model, it fits better to fluctuating signals. Under oscillations, it is not the same series of static phasor estimates than a series of dynamic ones. Estimates of the Fourier filter are poor under oscillations because the higher derivatives of the oscillation infiltrate into its estimates, as it was demonstrated in the theoretical and practical examples in [21, p. 808]. A kind of *Taylor aliasing*, in which, the higher derivatives excluded by the signal model have projections on the lower derivatives accepted in it, due to the non-orthogonality of

Taylor terms.

By extending its signal subspace to higher derivatives, the Taylor-Kalman filter is able to follow smooth fluctuations with better precision, by preventing the infiltration of the derivatives incorporated into its signal model. Of course, before abrupt changes, when much more higher derivatives are significant in the signal state, the Taylor-Kalman filter, as any dynamic system, will be characterized by its transient response. But between the subspace of the static state ($K = 0$) and the transient state ($K = \infty$), there is a series of subspaces that allocate much more room to the derivatives of smooth fluctuations, offering better estimates. This chapter discovers the advantages of the second ($K = 2$) subspace with respect to the static ($K = 0$) subspace.

In our view, the main conclusions of this chapter are doing is to create a new field of application for phasor estimation, much more appropriate to PMU applications. Its main contribution is to provide a new theoretical instrument for measuring the oscillations of a power system, in conditions that overshoot the precise boundaries of the relaying context.

2.7 Conclusions

State transition matrices are possible to represent Taylor approximations to the envelope of a power oscillation as a linear combination of the dynamic phasor and its first K derivatives. The Taylor-Kalman filter can be applied to power signals under oscillations to obtain much better instantaneous estimates of the dynamic phasor and its first derivatives, by its ability to follow smooth variations. The estimates achieved with the second order model reduce by a factor of ten the TVE error achieved with the zeroth-order model (traditional Kalman filter). The second-order filter is much more stable than the zeroth-order with settling times in the transient responses around five times lower (from twelve cycles to two cycles). The second-order filter improves also the zeroth-order phasor estimates in oscillations with frequency offset, with the advantage of providing frequency estimates together with the dynamic phasor estimates. Despite the shortcomings mentioned in the former section, these results open the way to new phasor estimation techniques using other kind of observers. The computational complexity of the estimator could also be reduced by exploiting the symmetry of the complex signal models. But the main advantage of these dynamic

phasor estimates, as compared with the Fourier filter ones is that, under oscillations, they are instantaneous (no delay at all) while they preserve their synchrony.

Chapter 3

Frequency Response of Taylor^K-Kalman-Fourier Filter for Instantaneous Oscillating Phasor Estimates

3.1 Introduction

Phasor estimation under dynamic conditions is an interesting research area today due to the proliferation of synchrophasor applications in wide area networks (WANs). It is also motivated by the increasing need not only of dynamic synchronized phasor measurements during oscillations, or severe system disturbances, but also of the power system frequency and its rate of change under those conditions. It is all the more important because the synchrophasor standard is under review to include the precedent dynamic aspects to the static signal model in which its phasor definition[9, Section 4.1] is based.

Phasor estimation under dynamic conditions was explored in [20]-[21] using the weighted least square (WLS) method leading to the Taylor-Fourier transform, which is more adequate under dynamic conditions than the traditional Discrete Fourier Transform (DFT), which is appropriate only for periodic signals with constant coefficients. The estimates of this method however contain a systematic delay. In order to solve this problem, the Kalman filter was proposed in [32]-[33] to estimate oscillating phasors, conducting to an instantaneous phasor estimator under these

conditions. But in these works the frequency response of the so called Taylor^K-Kalman filter was not taken into account. The purpose of this chapter is to show those frequency responses that help us to understand the behavior of the phasor estimates when the signals contain noise or components not contemplated into the signal model. At the same time, their interpretation will give us to an extended filter, the Taylor^K-Kalman-Fourier filter, that is able to perform the FFT or the Taylor-Fourier transform (TFT) with much less computation effort using the Kalman algorithm.

In phasor measurement applications the traditional Kalman filter has been used with a static signal model, i.e. assuming constant frequency, amplitude and phase. Its frequency response has been obtained separately for each state in [34], or for its real and imaginary parts in [27]. Their interpretation in both cases is difficult because, in the first case, you need to think in terms of two filters, and the procedure complicates when the number of states increases; and in the second case, you obtain two frequency responses, one for the real filter and the other for the imaginary one. So it is difficult to have an idea of the whole frequency response of the complex filter. On the other hand, the problem with [35] is that the illustrated frequency responses are obtained without freezing the Kalman gains, so it is hard to understand what a frequency response means in the case of an adaptive filter. Other papers refer to the frequency response of the Kalman filter but in other applications, such as [36], which makes a combination of the KF operating in the time domain and the Wiener filter in the frequency domain; or [37] that uses its time-frequency characteristics for tracking Multiple-Input Single-Output (MISO) systems for Orthogonal Frequency-Division Multiplexing (OFDM) applications; or [38], which smooths the spectra obtained through Fast Fourier Transform (FFT) with a Kalman filter. Finally, in [39] the design of navigation systems with multi sensors is described using the continuous time KF and classical frequency response techniques, such as Bode diagrams. So compared to the abundance of references on Kalman filter, the papers dealing with its frequency response are rather scarce, specially in our particular application.

The Taylor-Kalman filter proposed in [33] is based on a state-space signal model that incorporates derivatives of the complex envelope of the oscillation. With the advantage that it can estimate not only the phasor but also its derivatives. Its frequency response helps to assess the behavior of its estimates when the input signal has components not considered into the signal model. Its behavior in frequencies

other than the fundamental one can be improved by incorporating them into its signal model. We demonstrate here that it is possible to estimate the DFT or the TFFT with the Taylor-Kalman-Fourier filter, with the advantage of eliminating the delays implicit in their finite impulse response (FIR¹) filters.

Our investigation was motivated by the fact that there were several optimal solutions in phasor estimation such as Weighted Least Squares (WLS), Kalman, Shanks, etc. So our departing question was: what is the *optimum optimorum* from these methods? And our response now is that optimality depend basically on the signal subspace built by the method. For example, the subspace of the WLS solution is generated by vectors containing centered segments of the Taylor terms. They produce anticausal FIR filters. In the Shanks' case, the subspace is formed by the autoregressive and moving average (ARMA) causal vectors. The subspace of the Taylor-Kalman filter is generated by the state vector in the state-space signal model, which is also causal. In the last two cases, the responses are not implicitly delayed as in the first one.

The work in this chapter is based in the classical Kalman filter algorithm. Its main contribution is to provide its frequency response using the state transition matrix, and to show how it can be extended to the whole set of harmonics. It discusses how to do spectral analysis, including its derivatives, with the Kalman filter algorithm, with much less computational cost than the traditional FFT.

The chapter is organized as follows: in section 3.2, the state space signal model with its transition matrix and the Kalman filter equations are established. In section 3.3 the frequency response of the Taylor^K-Kalman filters are established and illustrated. Its extension to the full set of harmonics leads to the Taylor^K-Kalman-Fourier filter in section 3.4, in which its frequency response and numerical performance are compared with those of the FFT. Finally, phasor estimates of an oscillation with harmonics are discussed in section 3.5.

3.2 Signal Model and Kalman Filter

The signal model of the Taylor^K-Kalman filter comes from the Taylor approximation to the bandpass signal model proposed in [19] for power system oscillations. Its Kalman filter implementation was developed in [33]. In this section we make a

¹Finite Impulse Response.

reference to the algorithms illustrated in the previous sections 2.2 and 2.3.

3.3 Taylor-Kalman filter Frequency Response

The frequency response of the Taylor-Kalman filter can be obtained through the z transform of its update state equation

$$\hat{\mathbf{x}}(n) = \mathbf{\Phi}\hat{\mathbf{x}}(n-1) + \mathbf{K}(n)(s(n) - \mathbf{H}\mathbf{\Phi}\hat{\mathbf{x}}(n-1)) \quad (3.1)$$

with the steady-state Kalman gains in \mathbf{K} . The z -transform of (3.1) is

$$\hat{\mathbf{x}}(z) = \mathbf{\Phi}z^{-1}\hat{\mathbf{x}}(z) + \mathbf{K}(s(z) - \mathbf{H}\mathbf{\Phi}z^{-1}\hat{\mathbf{x}}(z)), \quad (3.2)$$

and solving for $\hat{\mathbf{x}}(z)$ we have

$$[\mathbf{I} - \mathbf{\Phi}z^{-1} + \mathbf{K}\mathbf{H}\mathbf{\Phi}z^{-1}] \hat{\mathbf{x}}(z) = \mathbf{K}s(z) \quad (3.3)$$

So the transfer functions between the states of the signal model and the input signal is given by

$$\mathbf{G}(z) = [\mathbf{I} + (\mathbf{K}\mathbf{H} - \mathbf{I})\mathbf{\Phi}z^{-1}]^{-1} \mathbf{K}, \quad (3.4)$$

and the frequency responses of the state filters are obtained evaluating the transfer functions in $\mathbf{G}(z)$ at $z = e^{j\theta}$, for $-\pi < \theta \leq \pi$.

3.3.1 Signal Test

To obtain the Kalman gains of the filters, a signal test of the form in (2.1) is built with the following amplitude and phase functions:

$$a(t) = a_0 + a_1 \sin(2\pi f_a t) \quad (3.5a)$$

$$\varphi(t) = \varphi_0 + \varphi_1 \sin(2\pi f_\varphi t) \quad (3.5b)$$

and the following parameters: $a_0 = 1$, $a_1 = 0.1$, and $f_a = 5\text{Hz}$, for the amplitude; and $\varphi_0 = 1$, $\varphi_1 = 0.1$, $f_\varphi = 5\text{Hz}$ for the phase. We also use the following parameters for the Kalman filter: $\sigma_v^2 = 0.01$ and $\sigma_w^2 = 10^{-4}$, which corresponds to a signal to noise ratio (SNR) of 37 dB.

3.3.2 Taylor⁰-Kalman Filter Frequency Responses

In Fig. 3.1 the frequency responses of the Taylor⁰-Kalman filter are shown for different sampling frequencies. Note that they are asymmetrical, indicating they pertain to complex filters. It is easy to see that when the input signal corresponds to a steady-state signal, it works appropriately with a gain equal to two at the positive fundamental frequency and zero at the negative one. They exhibit a resonance at the null frequency, indicating the presence of a pole close to $z = 1$ in the transfer function. The pole approaches more and more to one as the sampling frequency increases. It is well known that Kalman filter does not work appropriately when the input signal does not correspond to its signal model. In this case, the signal model corresponds to a rotatory signal with two components, one rotating at the fundamental frequency, and the other counter rotating. So the filter fails to extract a phasor from a constant signal, due to its non rotatory nature. The phase response is not zero flat at the fundamental frequency indicating a small delay in the estimates.

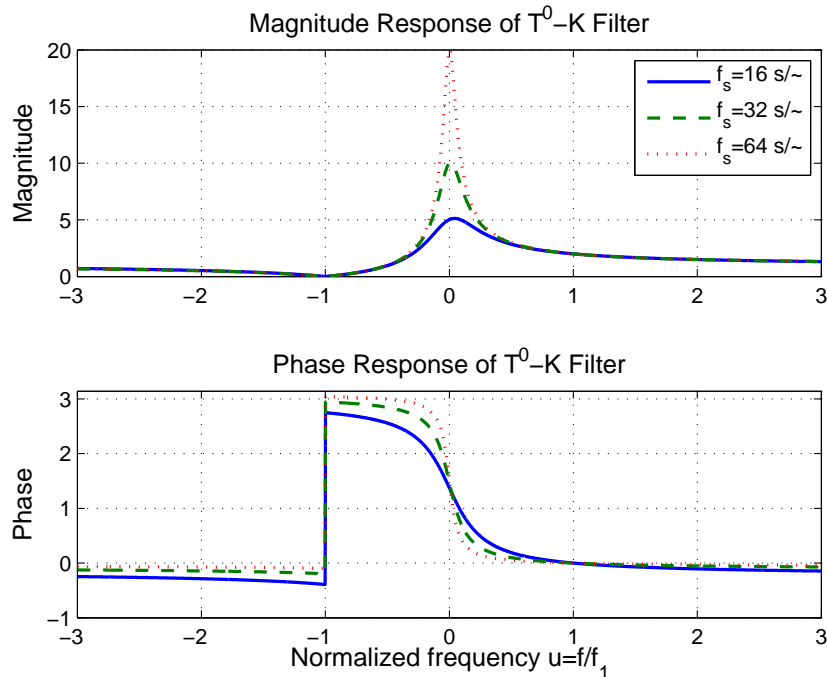


Figure 3.1: Frequency responses of the Taylor⁰-Kalman filter at different sampling frequencies.

The magnitude response of the Taylor⁰-Kalman filter illustrated in Fig. 3.1 is

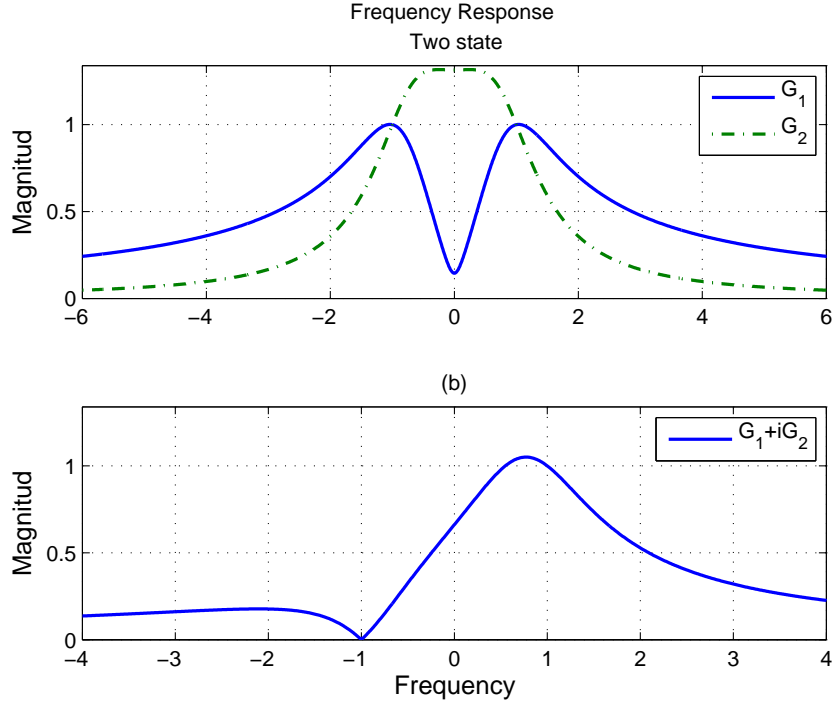


Figure 3.2: At the top, magnitude responses of Real and Imaginary parts of the Kalman filter as illustrated in [34] and at the bottom magnitude response of the complex gain.

equivalent to the one analyzed in [34, p. 103]. In that case, the variables of the state vector are the real and imaginary parts of the phasor. Using the parameters provided in that paper, we were able to reproduce the magnitude responses of the real and imaginary state variables in the top graph of Fig. 3.2. Note the similitude with those illustrated in Figs. 12-15 in [34]. The magnitude response (of the complex gain) built from the precedent ones is shown at the bottom. Note that it corresponds to a Taylor⁰-Kalman filter, but with its resonance slanted to the right, due to the different parameters of the examples. This corresponds also to the Kalman filter developed in [11, p. 102]. In that publication, it is demonstrated that before unknown initial conditions, and constant error covariance, Kalman filter estimates correspond exactly to those of the half-a-cycle Fourier filter. Since then, Kalman filter was silenced in the area of phasor measurement. However, note how different is the Kalman filter frequency response from that of the Fourier filter, which has the shape of a cardinal sine function. They only coincide in the two and zero gains at the positive and negative fundamental frequencies, respectively.

The resonance at the null frequency can be resolved by adding a zero at $z = 1$.

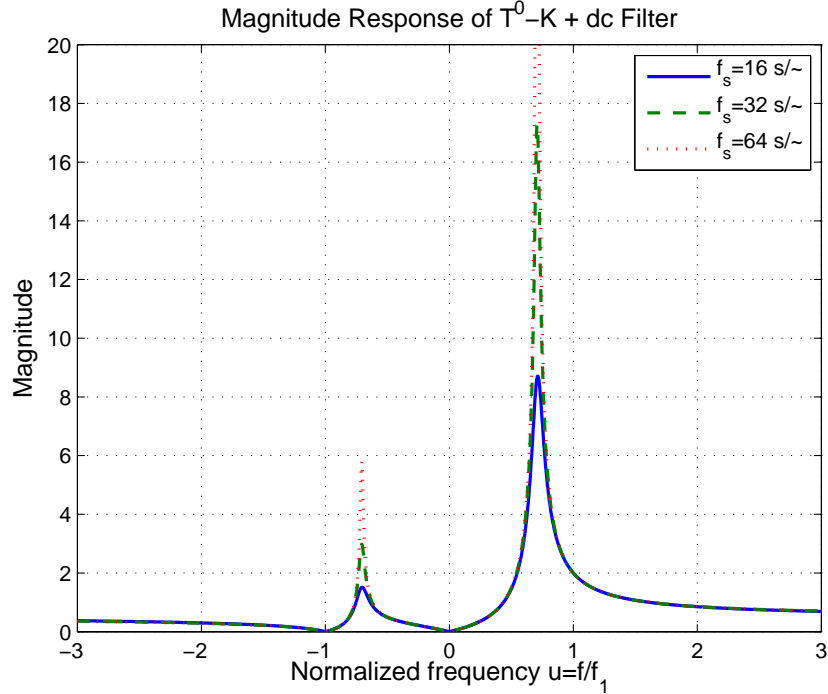


Figure 3.3: Magnitude responses of the Taylor⁰-Kalman-dc filter for different sampling frequencies.

This is achieved introducing a dc component to the rotatory signal model:

$$\Phi = \begin{pmatrix} 1 & 0 & 0 \\ 0 & \psi_1 & 0 \\ 0 & 0 & \bar{\psi}_1 \end{pmatrix}, \quad \mathbf{h} = \left(1 \quad \frac{1}{2} \quad \frac{1}{2} \right). \quad (3.6)$$

Note in Fig. 3.3 that its magnitude response has now a zero gain at the null frequency. In addition a lowpass filter is obtained from the first state variable (dc), its magnitude response is illustrated in Fig. 3.4. Note that it behaves as a low pass filter due to its flat gain at null frequency. These kind of filters are used in telecommunications to detect when the frequency of a signal goes out of a given interval.

3.3.3 Taylor²-Kalman Filter Frequency Response

The Taylor²-Kalman filter provides not only estimates of the phasor but also of the two first derivatives. Fig. 3.5 shows the magnitude and phase response of the phasor estimator filter. Note the flat gains around the fundamental frequencies (positive and negative). The filter exhibits again a resonance frequency close to the null frequency

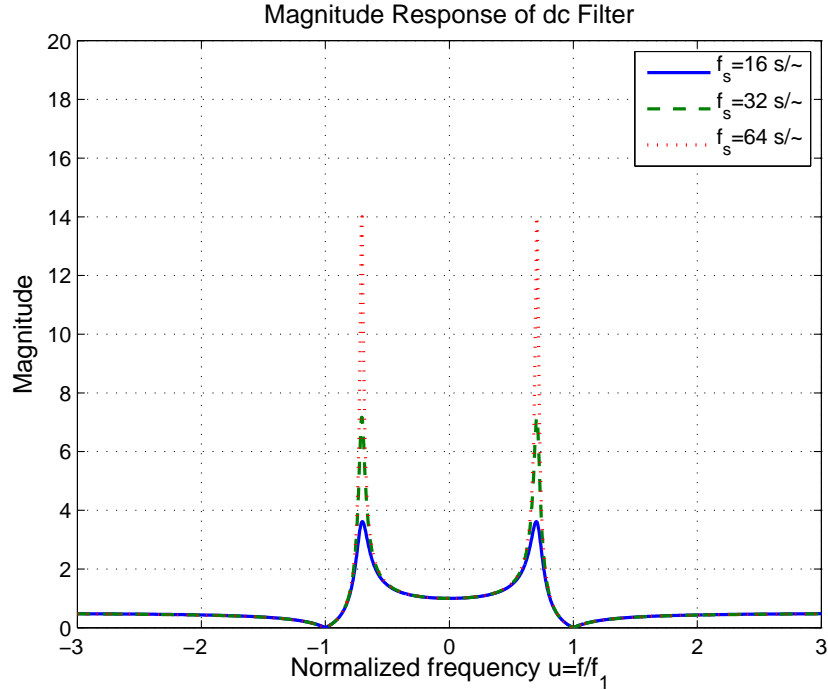


Figure 3.4: Magnitude responses of the dc filter for different sampling frequencies.

and has high gains at harmonic greater than one. So the filter works well only when the signal spectrum is confined into the intervals under the flat gains. The main feature of this filter is in its phase response. Note the null phase in the interval around the fundamental frequency, it means that the phasor estimates of this filter are instantaneous, i.e. without any delay when the spectrum of the oscillation is the bandpass signal assumed in our signal model. The abrupt phase change in the negative fundamental frequency is insignificant due to the null gain in that interval.

3.4 Taylor^K-Kalman-Fourier Filter

The precedent Taylor²-Kalman filter achieves ideal differentiator gains only around the fundamental frequency. To obtain those gains about every harmonic, the transition matrix of the signal model needs to be extended to all the harmonics of interest. For example, if the signal is sampled at $N = 2^\ell$ samples per period, and all of the harmonics are to be included, then the extended transition matrix is of the

when all the harmonics are included into the model, the frequency responses of the T^0 -K-F is the same of the DFT, and that of the T^2 -K-F filter, the same of the T^2 -F transform without delay. So the T^0 -K-F filter implementation is a faster algorithm to do harmonic analysis than the famous FFT.

3.4.1 Taylor⁰-Kalman-Fourier Filter

Our first example is the Taylor⁰-Kalman-Fourier filter for a sampling frequency of $N = 16$ samples per cycle. Its transition matrix is a diagonal matrix with the phase rotating factors $\{\psi^k, k = 0, 1 \dots, 15\}$ descending through the diagonal. Its frequency response is plotted in Fig. 3.6 together with the frequency response of the one-cycle Fourier filter. Note that they are exactly the same, and indicates that the Taylor⁰-Kalman-Fourier (T^0 -K-F) allows the calculation of the DFT with the Kalman algorithm. Note in its phase response that estimates of the Taylor⁰-Kalman-Fourier will have exactly the same delay as those of the one-cycle Fourier filter, which is a half a cycle.

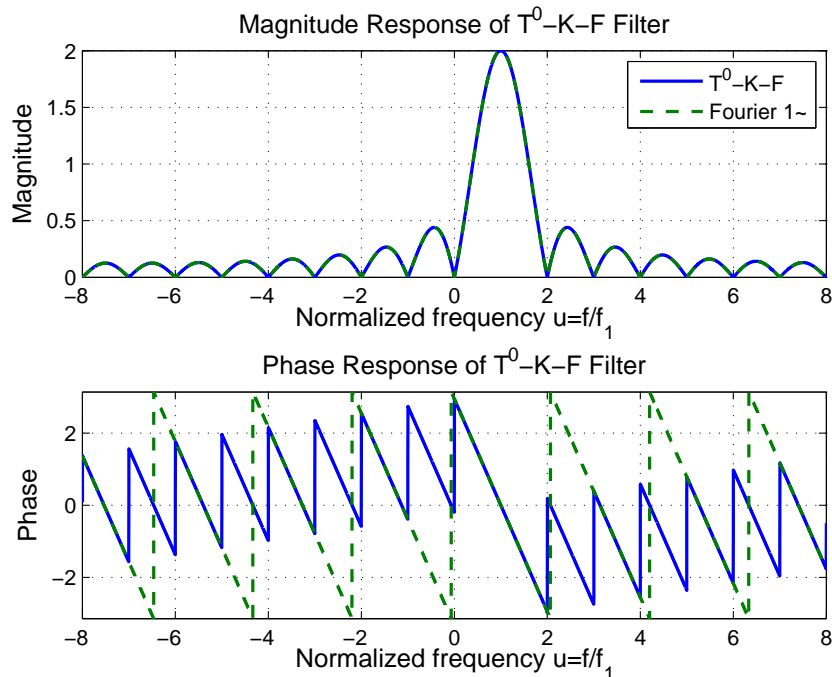


Figure 3.6: Frequency response to the $T^0 - K - F$ filter.

3.4.2 Taylor²-Kalman-Fourier Filter

The second example is the Taylor²-Kalman-Fourier filter. Now its transition matrix has in its diagonal the submatrix Φ_2 multiplied by the phase rotating factors $\{\psi^k, k = 0, 1 \dots, 15\}$.

Fig. 3.7 shows the magnitude and phase response of the T²-K-F filter of the first harmonic. The magnitude appears together with the response of the one-cycle Fourier filter to appreciate the transformation due to the change from the zero to two in the order of the Taylor polynomial. The comb filter is transformed into a fence filter, i. e. a filter that extracts one oscillating harmonic, rejecting the rest of harmonics. Note that despite of the widening and increase of the mainlobe and sidelobe levels, the gains in the harmonic bands improve a lot because of their flatness. Those gains improve the filtering by avoiding the magnitude and phase distortion at the harmonic of interest and by having a better rejection of the rest of harmonics. Note in the phase response that the phase under the passband is a zero flat, indicating no delay in the phasor estimates. This means that phasor estimates can be truly synchronized with a time stamp in the nanosecond scale. A huge advantage of these estimates, extremely useful for control applications. In the next section we demonstrate this fact in a numerical example. With the second-order Taylor signal model is also possible to obtain estimates of the first and second derivatives of the oscillation. Fig. 3.8, shows the magnitude responses for the first and second phasor derivatives respectively. Note that close to the fundamental frequency the magnitude responses exhibit the ideal differentiator gains (line and parabolic shapes).

Before going to the numerical example, a few words about subspaces. The development of the Taylor^K-Kalman-Fourier filter by including one by one the full set of harmonics shows that the subspace of the Taylor⁰-Kalman filter, whose frequency response is illustrated in Fig. 3.1, grows little by little until reaching the full Fourier subspace, with the frequency response illustrated in Fig. 3.6; or that of the Taylor²-Kalman filter in Fig. 3.5 with that of Fig. 3.7. That is why it is possible to perform the DFT with the T⁰-K-F, and T²-F transform with the T²-K-F filter, without the delay of the FIR filters.

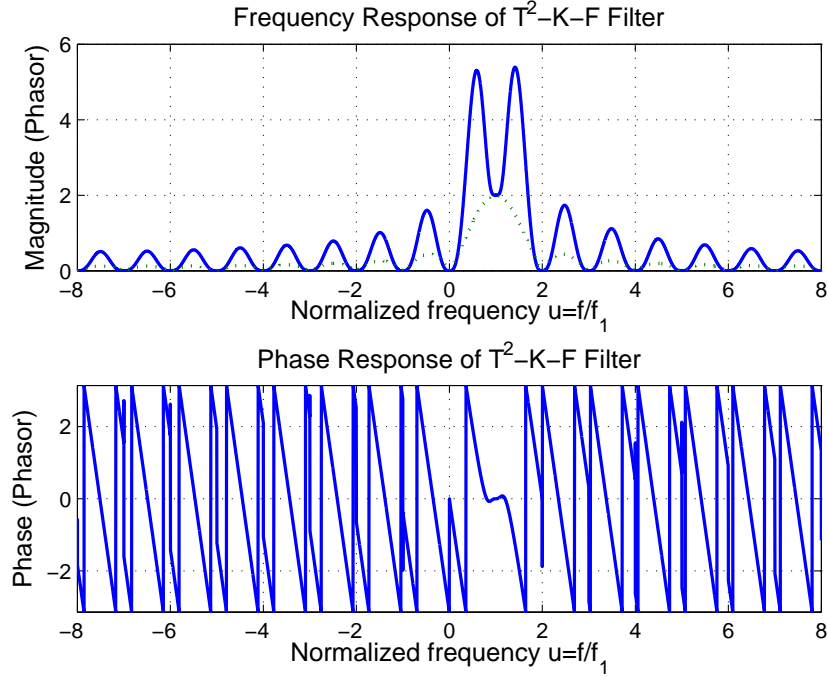


Figure 3.7: Frequency response to the $T^2 - K - F$ filter.

3.5 Numerical Results

In this section we test the T^0 -K-F and the T^2 -K-F filters with an oscillatory signal to which a 3rd and 5th harmonics are added at a certain instant of time. The signal is sampled at $N = 64$ samples per fundamental cycle. The performance on phasor estimation of those filters using $N = 64$ harmonics is analyzed.

Test Signal

$$\begin{aligned}
 s(t) = & a(t)\cos(2\pi f_1 t + \varphi(t)) \\
 & + u(t) \left[\frac{a(t)}{10} \cos(2\pi 3f_1 t + \varphi_3(t)) \right. \\
 & \left. + \frac{a(t)}{20} \cos(2\pi 5f_1 t + \varphi_5(t)) \right]
 \end{aligned} \tag{3.9}$$

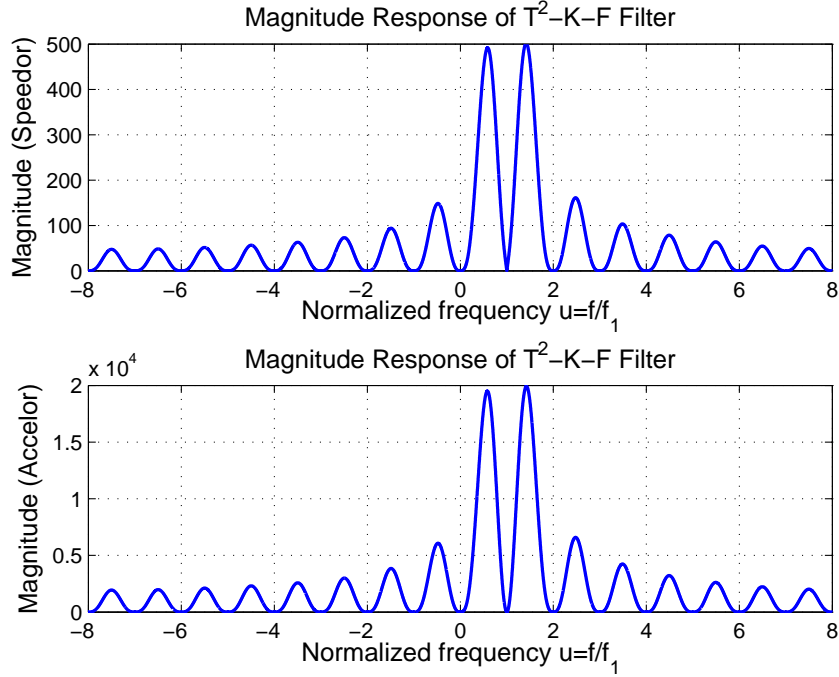


Figure 3.8: Magnitude response of the first and second differentiators associated with the T²-K-F filter.

where

$$u(t) = \begin{cases} 0, & \text{for } t < 15/f_1 \\ 1, & \text{for } t \geq 15/f_1 \end{cases} \quad (3.10)$$

$$a(t) = a_0 + a_1 \sin(2\pi f_a t) \quad (3.11)$$

$$\varphi(t) = \varphi_0 + \varphi_1 \sin(2\pi f_\varphi t) \quad (3.12)$$

$$\varphi_3(t) = 0.9\varphi(t) \quad (3.13)$$

$$\varphi_5(t) = 0.8\varphi(t) \quad (3.14)$$

and the following parameters in amplitude: $a_0 = 1$, $a_1 = 0.1$, $f_a = 5Hz$; and phase, $\varphi_0 = 1$, $\varphi_1 = 0.1$, $f_\varphi = 5Hz$. The noise variances in the Kalman filter are: $\sigma_v^2 = 0.01$ and $\sigma_w^2 = 10^{-4}$.

The test signal and its estimates are illustrated in Fig. 3.9. As you can see in (3.10), the injection of the harmonics starts at the 15th cycle. Signal estimates are very good for both filters, that is why no differences between the three curves are perceptible. It is well known that Kalman filter is good when the input signal corresponds to its model. The estimation error (bottom graph) indicates however a

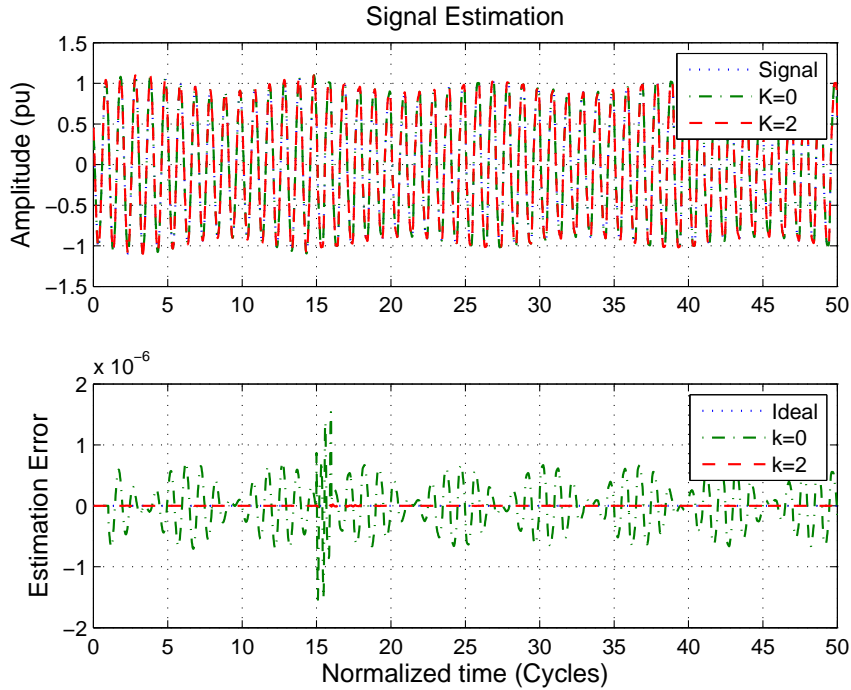


Figure 3.9: Signal and error estimates.

higher error for the T^0 -K-F filter with an important transient immediately after the harmonic injection instance. But we are using Kalman filter to estimate not the input signal but its phasor. In the left column of Fig. 3.10, the phasor estimates obtained with both filters are shown. The T^0 -K-F filter produces estimates with a perceptible corrugated shape, and delayed half a cycle from the smoother estimates obtained with the T^2 -K-F filter. These estimates are closer to the ideal phasor, except at the transient occurring immediately after the injection of the harmonics, due to the discontinuity of their step change when they appear. This is a very important result, that shows that the zero Taylor polynomial model is unable to suppress the delay in the estimates, and the second order Taylor polynomial together with the Kalman filter algorithm produces instantaneous estimates that can be truly synchronized with a precise time stamp. Finally, the first derivative estimates obtained with the second order Taylor filter are shown in the right column of Fig. 3.10. These estimates are not so good as the phasor estimates but they could be improved by using a model of higher order.

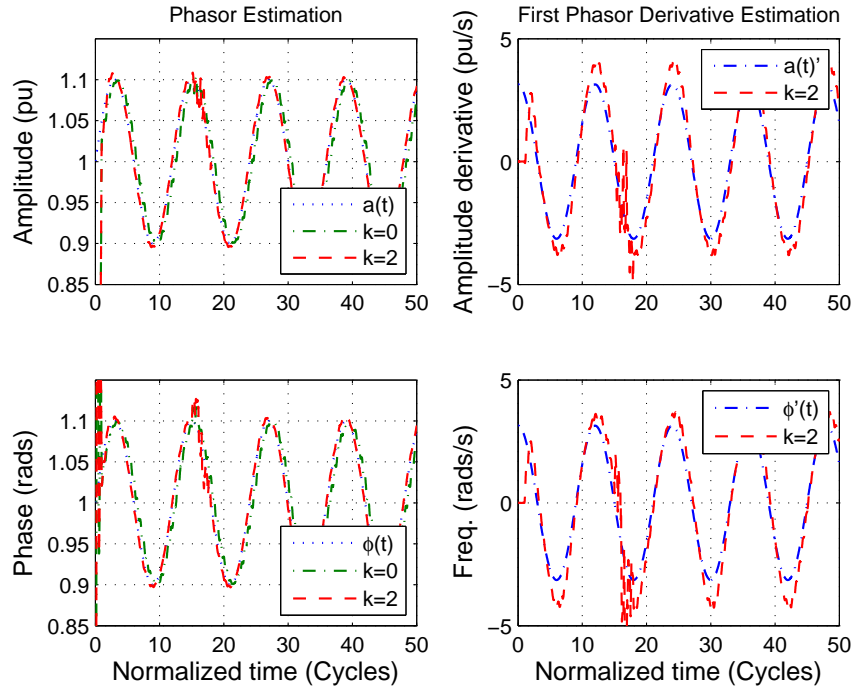


Figure 3.10: At the left, phasor estimates with the zeroth and 2nd order Taylor models and at the right first derivative estimates with $K = 2$.

3.6 Conclusions

Frequency responses of the Taylor^K-Kalman filter developed in the first part of the chapter indicate that this filter is very sensitive to noise and that its good performance in phasor estimation depend on the concurrence of the input signal with its signal model. The extension of the signal model to the full set of harmonics lead to the Taylor^K-Kalman-Fourier filter. It was shown that Taylor⁰-Kalman-Fourier filter has the same performance in harmonic analysis as DFT, but with much less computational burden, even than in its FFT implementation. On the other hand, the Taylor²-Kalman-Fourier filter is a fence filter able to perform in real time the Taylor²-Fourier transform, but with much less computational effort; and most importantly, without delay. The inclusion of a second order Taylor polynomial in the signal model achieves a flat magnitude and phase response about every harmonic producing harmonic oscillating phasor estimates without magnitude or phase distortion (no delay). These instantaneous estimates can be truly synchronized to the microsecond time scale, and therefore are very useful for control applications of the power system.

Chapter 4

Taylor^K-Kalman-Fourier Differentiators for Instantaneous Derivative Estimates

4.1 Introduction

Digital differentiators are very useful in signal processing, monitoring [40]-[42], and control [43]-[45] applications. In some applications derivatives are more important than the signal itself. Such is the case, for example, of the speed estimator of a target in a radar, or the estimation of the frequency variations on a power system under oscillations. One of the most popular implementations of digital differentiators is using a finite impulse response (FIR) filter [46]. The problem of estimates obtained with linear phase FIR filters is that they have inevitable delay, by half the length of its impulse response. Such is the case of the Parks-McClellan implementation [47], or the filter bank of maximally flat differentiators recently proposed in [48].

Other well known FIR implementations can be found in [49], in the case of low-pass filters designed with the maximally flat criterion, or [50] -[54] in the case of full-band differentiators. In [55] digital linear-phase differentiators are designed based on a relationship between the coefficients of a digital differentiator and those of the generic fractional delay filter. And finally, in [56], the interrelationships between the digital differentiator, the digital Hilbert transformer (DHT), and the half-band low-pass filter are established.

Even if a systematic delay is not a problem in communications applications,

which are always delayed at least one symbolic period, this anomaly exclude the FIR implementation from control applications, due to the potential instability provoked by a delay in the control loop. In this case, instantaneous estimates are preferable. This is achieved with digital differentiators implemented with infinite impulse response (IIR) filters. These filters use much less coefficients than the equivalent FIR filters, but they have non-linear phase response, because they are causal or time asymmetrical. This means they produce phase and amplitude distortion. Such is the case of the full-band IIR differentiators designed in [57] based on the formulation of a generalized eigenvalue problem using the Remez multiple exchange algorithm, or the low-pass IIR digital differentiators in [58], whose numerators have a predominant linear phase, at least over the frequency interval of operation.

Observers can be classified as another kind of digital differentiators, even if they also provide IIR filters. The problem with observers of dynamic systems is they estimate the state space variables of a dynamic system, which not necessary coincide with the derivatives of the output signal of interest. One of the most common observers is the Kalman filter. In [59] the conditions for obtaining the first derivatives of a dynamic system with the Kalman algorithm when the state space equations of the system are known. This method achieves an optimum differentiator, which obtains the minimum variance unbiased estimates of the first derivatives in the state vector of a known dynamic system.

In this work, we present other set of optimum digital differentiators that do not require at all *a priori* knowledge of any dynamic system. Instead, the Kalman algorithm is applied to approach a signal with its Taylor signal model, expressed by a state transition matrix that depends only on the sampling time, and the desired order of the Taylor polynomial. The subspace generated by this signal model is similar to the one developed in [48]. But instead of obtaining the derivative estimates through the least squares (LS) method, which leads to FIR filters, we use the Kalman filter to project the input signal into the Taylor signal model subspace. We are going to show that for Taylor orders greater than, or equal to two, the achieved frequency responses are very close to those of the ideal differentiators on the frequency baseband, which in turn means instantaneous and undistorted estimates, provided the spectrum of the input signal be on that band. The filters achieved with this method are referred to as Taylor^K-Kalman (T^K-K) filters. Their problem is that they have lateral high gains, or high sensitivity to noise. But that gain can be mitigated by extending

the signal model through the inclusion of harmonic components. This extended solution leads to the Taylor^K-Kalman-Fourier (T^K-K-F) filters proposed in [33] for instantaneous oscillating phasor estimates. With this method is possible to estimate the digital Fourier transform (DFT) with the Kalman Algorithm using a zeroth-order Taylor polynomial, with much less computational effort than that of the fast Fourier transform (FFT). It is also possible to estimate the Taylor^K-Fourier transform proposed in [21] by increasing the order of the Taylor polynomial.

The main goal of our investigation was to find an unifying theory for obtaining the best derivative estimator through the many options available today: least squares, Kalman filter, maximum likelihood, etc. Our initial question was to find the best among the best, or the *optimum optimorum*. Here, we use the traditional Kalman algorithm. So, our main contribution consists in expressing the Taylor signal model in terms of a state transition matrix, so the traditional Kalman algorithm can be applied over one, or the whole set of harmonic frequencies. And, of course, to find a method able to provide instantaneous and undistorted estimates of the first derivatives of a signal, provided its spectral load be over the frequency intervals under flat magnitude and phase response of the differentiators.

The spectral condition of the differentiator ideal operation corresponds to oscillating signals. The derivative estimates are good in time intervals where the oscillation is smooth and without discontinuities. We develop the frequency response of the filters to assess the behavior of the estimates when the signal contains discontinuities or noise. The order of the Taylor polynomial can be increased, but there is a limit imposed by the size of the sampling time, because the elements of the state transition matrix are integer powers of this parameter, so for high sampling frequencies, they vanish. But with an order of three it is already possible to estimate position, speed and acceleration.

The chapter is organized as follows: in section 4.2 shows the Taylor^K-Kalman differentiators, the state space signal model by differentiators is defined and the frequency responses of the Taylor^K-Kalman differentiators, in section 4.3 the mitigation of the high gain with the low-pass Taylor^K-Kalman differentiator is illustrated. In section 4.4 the T^K-K-F filter is developed and an example of frequency response is illustrated. Finally in section 4.5 the main results using a second-order and third-order differentiators are presented and discussed.

4.2 Taylor^K-Kalman Differentiators

In this section we develop the three components of the Taylor^K-Kalman differentiators. First, we introduce the Taylor signal model represented in state space equations. Its state transition matrix makes possible the use of the Kalman algorithm. Finally, we develop the equations for obtaining the frequency responses.

4.2.1 Taylor Signal model

Let $s(t)$ be a signal with up to its K th derivative continuous in the time interval $\mathcal{T} = \{t : |t - t_0| < T_m\}$, with Taylor interval of size T_m . It is always possible to approach it in that interval by a K th-order Taylor polynomial centered at t_0 :

$$s_K(t) = s(t_0) + \dot{s}(t_0)(t - t_0) + \dots + s^{(K)}(t_0) \frac{(t - t_0)^K}{K!}$$

$$t_0 - \frac{T_m}{2} \leq t \leq t_0 + \frac{T_m}{2} \quad (4.1)$$

By successively differentiating $s_K(t)$ in (4.1) as follows:

$$\begin{aligned} s_K(t) &= s(t_0) + \dot{s}(t_0)\tau + \ddot{s}(t_0)\frac{\tau^2}{2!} + \dots + s^{(K)}(t_0)\frac{\tau^K}{K!} \\ \dot{s}_K(t) &= \dot{s}(t_0) + \ddot{s}(t_0)\tau + \dots + s^{(K)}(t_0)\frac{\tau^{K-1}}{(K-1)!} \\ &\vdots \\ s_K^{(K)}(t) &= s^{(K)}(t_0) \end{aligned} \quad (4.2)$$

with $\tau = t - t_0$. And by defining the state vector $\mathbf{s}_K(t)$, with the first K derivatives of the Taylor signal model $s_K(t)$, we see that (4.2) can be written in matrix form as:

$$\mathbf{s}_K(t) = \mathbf{\Phi}_K(\tau)\mathbf{s}_K(t_0) \quad (4.3)$$

in which $\mathbf{\Phi}_K(\tau)$ is the state transition matrix between t_0 and t :

$$\mathbf{\Phi}_K(\tau) = \begin{pmatrix} 1 & \tau & \frac{\tau^2}{2!} & \dots & \frac{\tau^K}{K!} \\ & 1 & \tau & \dots & \frac{\tau^{K-1}}{(K-1)!} \\ & & 1 & \dots & \frac{\tau^{K-2}}{(K-2)!} \\ & & & \ddots & \vdots \\ & & & & 1 \end{pmatrix}. \quad (4.4)$$

note that is the same matrix in 2.6 but without the phase rotation factor ψ_1 .

Under this representation, the Taylor signal model is then given by:

$$s_K(t) = \mathbf{h}^T \mathbf{s}_K(t) \quad (4.5)$$

where $\mathbf{h}^T = \begin{bmatrix} 1 & 0 & \dots & 0 \end{bmatrix}$, with K zeros.

Finally, assuming $t_0 = (n-1)T$ and $t = nT$, where T is the sampling period, we have the following discrete state transition equation:

$$\mathbf{s}_K(n) = \mathbf{\Phi}_K(T) \mathbf{s}_K(n-1) \quad (4.6)$$

In the next section, we show how these signal model can be used in the Kalman filter to estimate the derivatives contained in the state vector from a given signal. Once the Kalman filter reaches its steady-state gains, it will decompose the input signal $s(t)$ into the state-vector components of the signal model $s_K(t)$.

4.2.2 Differentiator Frequency responses

The frequency response of the Taylor-Kalman filter can be obtained through the z transform of its update state equation

$$\hat{\mathbf{x}}(n) = \mathbf{\Phi} \hat{\mathbf{x}}(n-1) + \overline{\mathbf{K}}(s(n) - \mathbf{H} \mathbf{\Phi} \hat{\mathbf{x}}(n-1)) \quad (4.7)$$

with the steady-state Kalman gains in $\overline{\mathbf{K}}$. The z -transform of (4.7) is

$$\hat{\mathbf{x}}(z) = \mathbf{\Phi} z^{-1} \hat{\mathbf{x}}(z) + \overline{\mathbf{K}}(s(z) - \mathbf{H} \mathbf{\Phi} z^{-1} \hat{\mathbf{x}}(z)), \quad (4.8)$$

and solving for $\hat{\mathbf{x}}(z)$ we have

$$[\mathbf{I} - \mathbf{\Phi} z^{-1} + \overline{\mathbf{K}} \mathbf{H} \mathbf{\Phi} z^{-1}] \hat{\mathbf{x}}(z) = \overline{\mathbf{K}} s(z). \quad (4.9)$$

So the transfer functions between the states of the signal model and the input signal are given in the following polynomial vector:

$$\mathbf{G}(z) = [\mathbf{I} + (\overline{\mathbf{K}} \mathbf{H} - \mathbf{I}) \mathbf{\Phi} z^{-1}]^{-1} \overline{\mathbf{K}} \quad (4.10)$$

and the frequency responses are obtained evaluating $\mathbf{G}(z)$ at $z = e^{j\theta}$, for $-\pi \leq \theta \leq \pi$.

4.2.3 Taylor²-Kalman Differentiator Frequency response

Fig. 4.1 shows the magnitude and phase responses of the zeroth derivative (position) estimates of the T²-K differentiators. The responses are shown for different sampling frequencies measured in samples per fundamental period, assuming a fundamental frequency of $f_1 = 50\text{Hz}$. Note that both responses are flat about the null frequency, corresponding to the gain of an ideal signal estimator. If the spectrum of the input signal is confined under the flat frequency response, approximately $0.2f_1 = 10\text{Hz}$, then the filter will not distort the signal, neither in magnitude nor in phase. This means that, provided the signal spectrum be confined in the ideal operation frequency band, the estimates are not delayed (instantaneous) or attenuated at all. The magnitude response of the first and second derivative (speed and acceleration) estimators are shown in Fig. 4.2. Note again that, in the neighborhood centered at the zero frequency, they have the gains of the corresponding ideal differentiator, diverging with high constant values outside the ideal operation band. The corresponding phase responses are shown in Fig. 4.3. They also approach the ideal differentiator phase responses ($j\omega$ and $(j\omega)^2$) close to the null frequency. There, they approach a Sign function of size π and 2π in frequency corresponding to the j and j^2 factors. So, derivative estimates are also instantaneous. Then, they operate as ideal differentiators when the input signal spectrum is confined inside the ideal operation frequency band. In the time counterpart, it means that they operate as ideal differentiators when the input signal is clean of noise and sufficiently smooth as to be approached with enough precision by a second-order Taylor polynomial.

4.3 Low-Pass Taylor^K-Kalman Differentiator

One way to mitigate the high gains of the T^K-K differentiator consists in extending the transition matrix in (4.4) by including a new angular frequency component at $e^{j\pi}$, corresponding to the half-band frequency. The incorporation of the first derivatives of the complex envelope at this frequency will be seen from the dc component (e^{j0}) as an extraction, so the gain of the low-pass differentiators will go down in the half-band. These filters will be referred to as low-pass Taylor^K-Kalman (LP T^K-K) differentiators . The new transition matrix will be:

$$\Phi(T) = \begin{pmatrix} \Phi_K(T) & \\ & \Phi_K(T)e^{j\pi} \end{pmatrix} \quad (4.11)$$

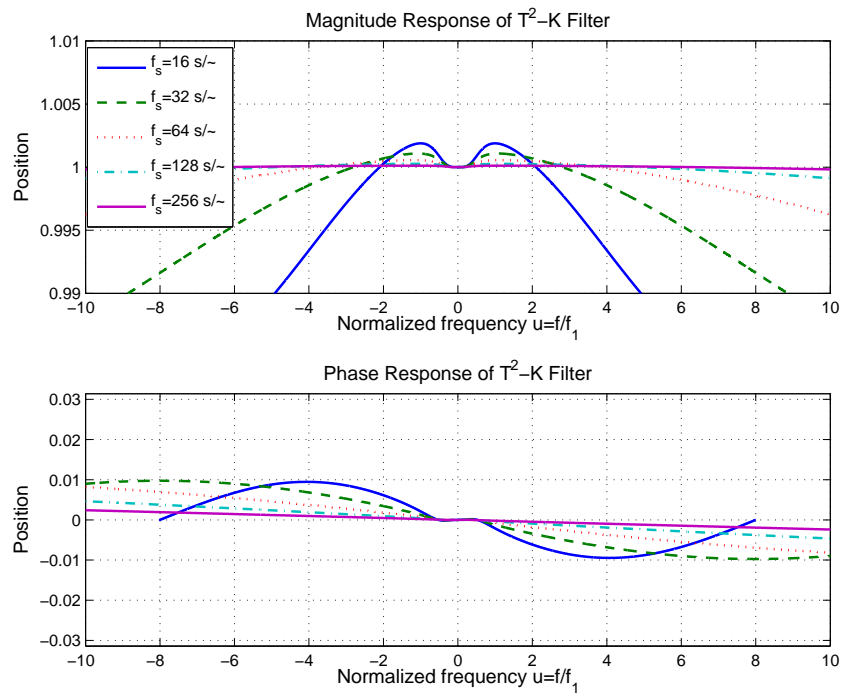


Figure 4.1: Magnitude and phase response of the zeroth T^2 -K differentiator. The frequency response is flat around the null frequency.

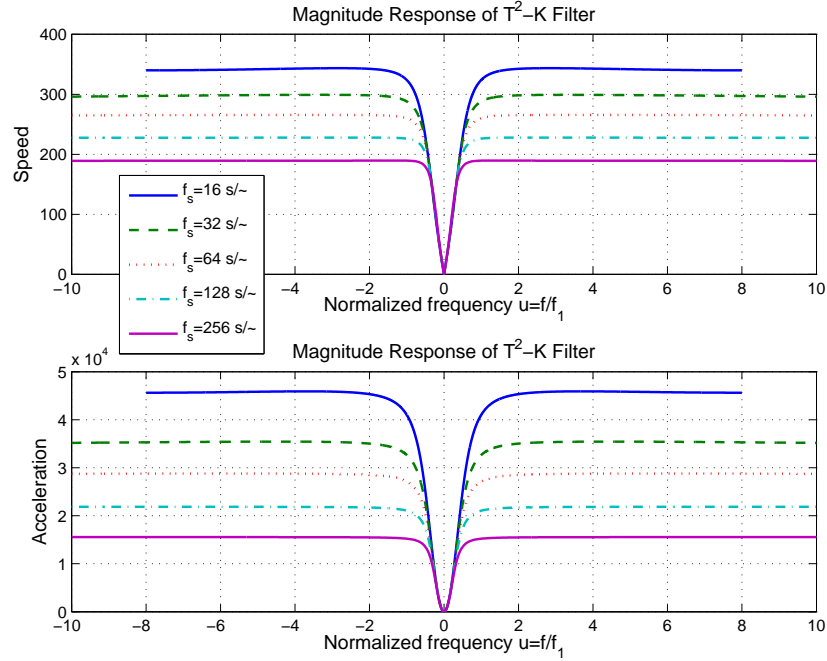


Figure 4.2: Magnitude response of the first and second T^2 -K differentiators. Note the linear and parabolic gains around the null frequency.

with the following state transition equation

$$\mathbf{s}_K(n) = \Phi(T) \mathbf{s}_K(n-1) \quad (4.12)$$

and the signal model

$$s_K(n) = \mathbf{H} \mathbf{s}_K(n) \quad (4.13)$$

where $\mathbf{H} = (\mathbf{h}^T \mathbf{h}^T)$, because $\mathbf{s}_K(t)$ contains now also the derivatives of the half-band frequency.

Fig. 4.4 shows the frequency response of the zeroth compensated differentiator. Note that now the gain goes down to a flat zero at the halfband frequency, while the flat frequency response close to the null frequency is preserved. This effect appears completely illustrated only for the case of the lower sampling frequency, but it happens for all. The same holds for the first and second differentiator frequency responses illustrated in Figs. 4.5 and 4.6.

In the next section, the transition matrix will be extended to the whole set of harmonic frequencies to obtain the T^K -Kalman-Fourier differentiators.

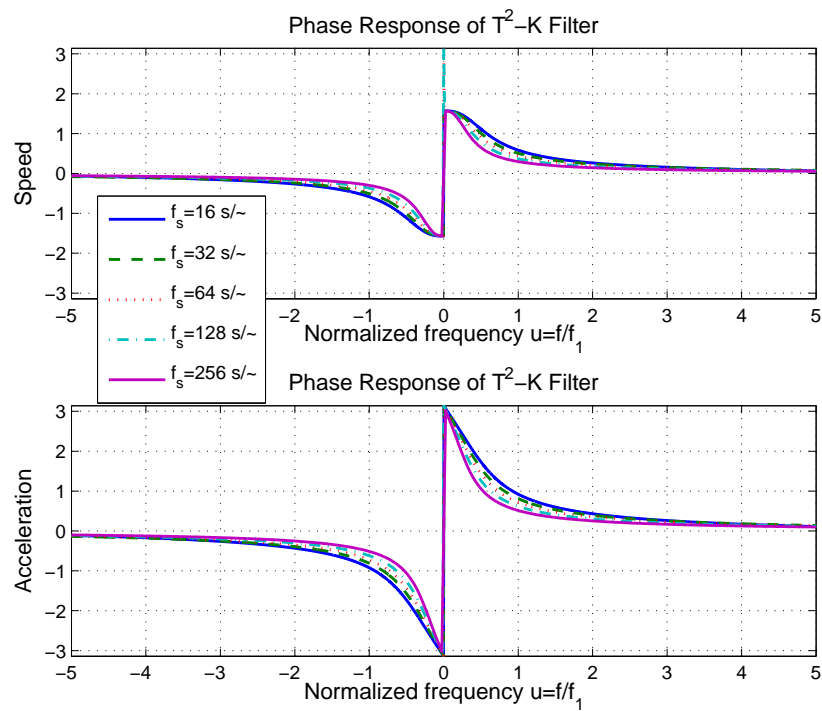


Figure 4.3: Phase response of the first and second T^2 -K differentiators. Close to the zero frequency, they have the ideal phase responses $(j\omega)$, and $(j\omega)^2$.

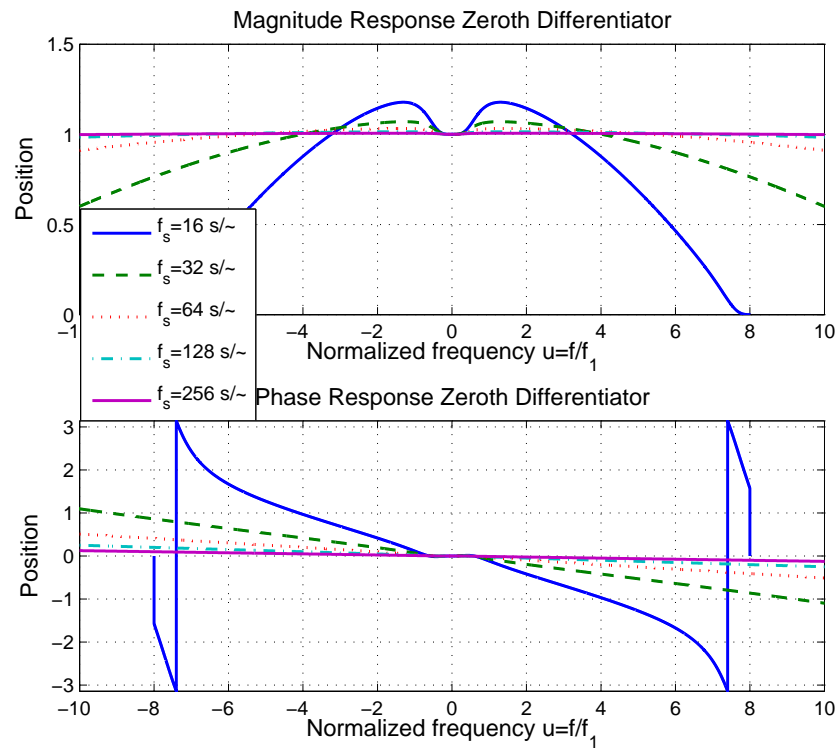


Figure 4.4: Magnitude and phase response of the zeroth LP T^2 -K differentiator.

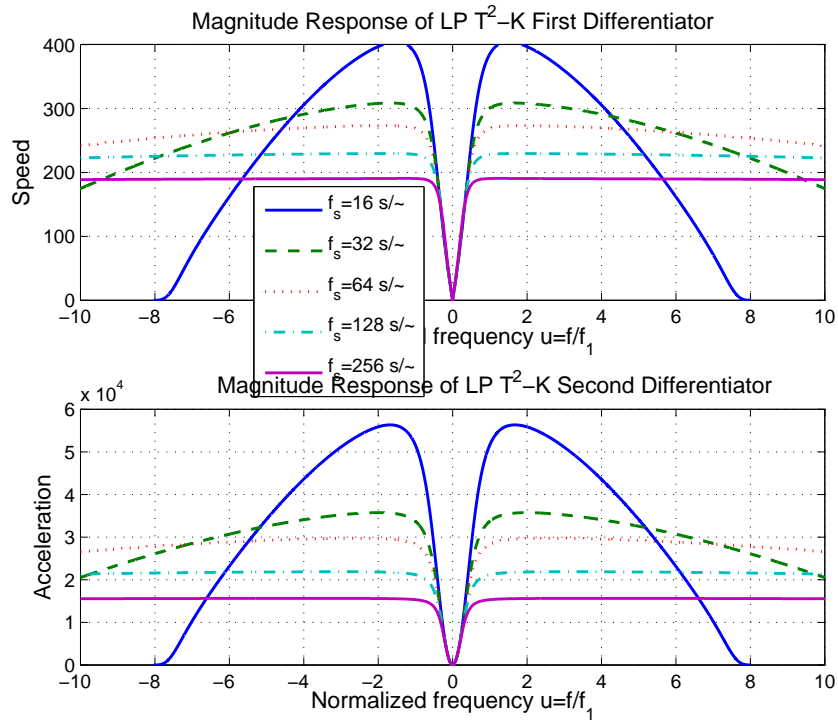


Figure 4.5: Magnitude response of the first and second LP T^2 -K differentiators.

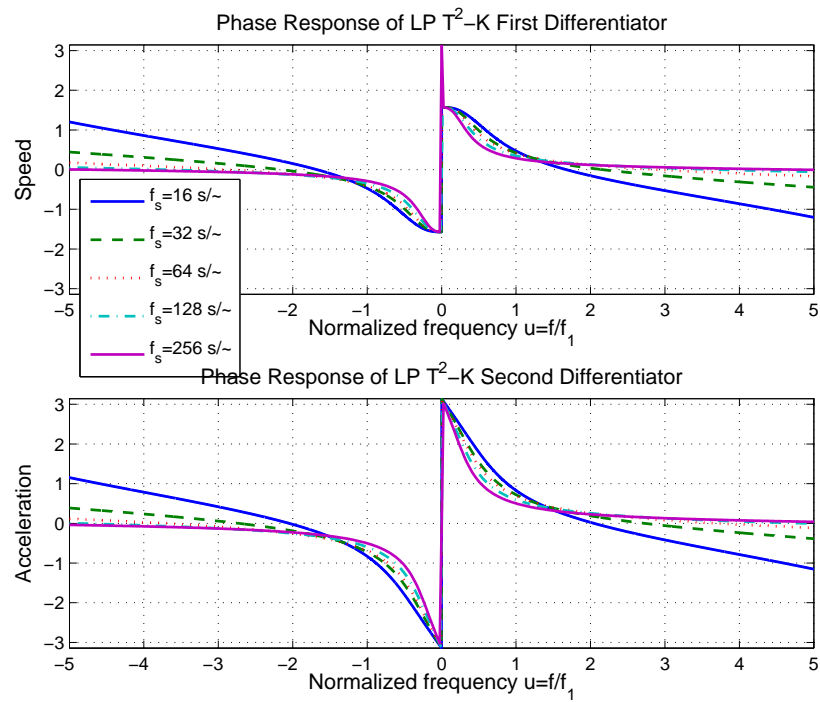


Figure 4.6: Phase response of the first and second LP T^2 -K differentiators.

4.4 Taylor^K-Kalman-Fourier Differentiators

The state transition matrix can be extended to the full set of harmonic frequencies. These differentiators will be referred to as *Taylor^K-Kalman-Fourier* differentiators, because they can estimate the first derivatives of the complex envelope at each harmonic frequency. This bank of filters was first proposed in [33] and can also be seen as a Taylor extension of the digital Fourier transform (DFT).

The extended state transition matrix is now:

$$\Phi(T) = \begin{pmatrix} \Phi_K(T) & & & \\ & \Phi_K(T)\psi^1 & & \\ & & \ddots & \\ & & & \Phi_K(T)\psi^{N-1} \end{pmatrix} \quad (4.14)$$

with $\psi = e^{j\frac{2\pi}{N}}$ for a sampling frequency of Nf_1 . The size of the state transition matrix is $(K + 1) \times N$. The state vector contains the derivatives of the whole set of harmonics and its output vector is:

$$\mathbf{H} = \begin{bmatrix} \mathbf{h}_1^T & \mathbf{h}_2^T & \dots & \mathbf{h}_N^T \end{bmatrix}. \quad (4.15)$$

with a size of $1 \times (K + 1)N$, therefore N row vectors defined by $\mathbf{h}^T = [1 \ 0 \ \dots \ 0]$, with K zeros.

The magnitude response of the T²-K-F differentiators including 32 harmonics is shown in Fig. 4.7. Note that now the gain of all the differentiators goes down as the frequency increases, ensuring full rejection with flat null gain at every harmonic frequency. The phase responses are illustrated in Fig. 4.8. It can be seen that ideal phase responses are preserved around the null frequency. The illustrated case corresponds to a sampling frequency of 32 samples per cycle. But the main advantage of the estimates is that they are instantaneous, as it can be confirmed by the phase responses close to the zero frequency.

Another advantage of this filter bank is that the first derivatives of the full set of harmonic frequencies can be obtained at once. If the signal spectrum is confined in the ideal operation interval, then the differentiators operate a digital transformation, mapping the signal into the first derivatives of the complex envelope of each harmonic frequency. In the next section we consider numerical examples.

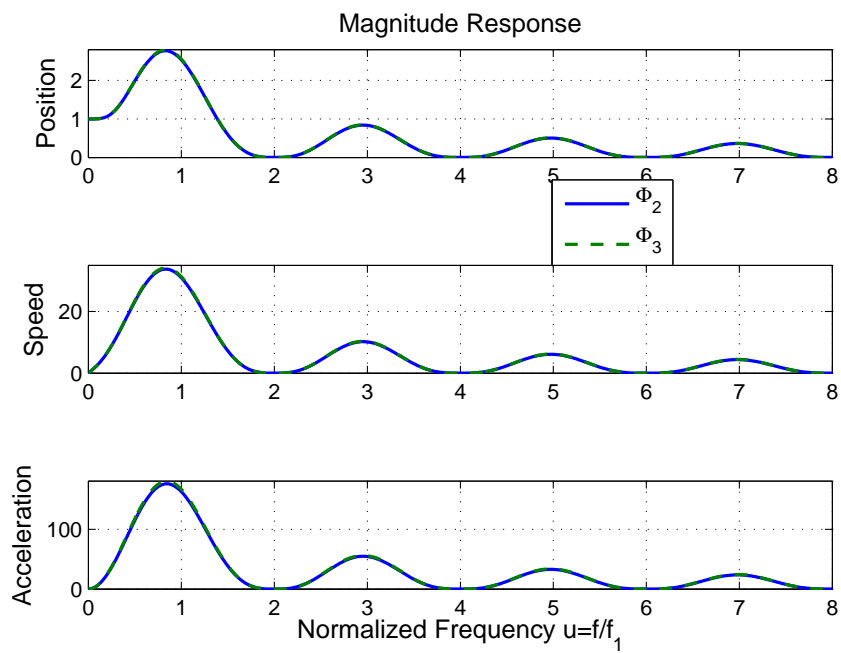


Figure 4.7: Magnitude response of the first three Taylor^K-Kalman-Fourier differentiators for $K = 2, 3$, and 32 harmonics. Note that ideal differentiator gains are achieved about null frequency and full rejection about harmonic frequencies.

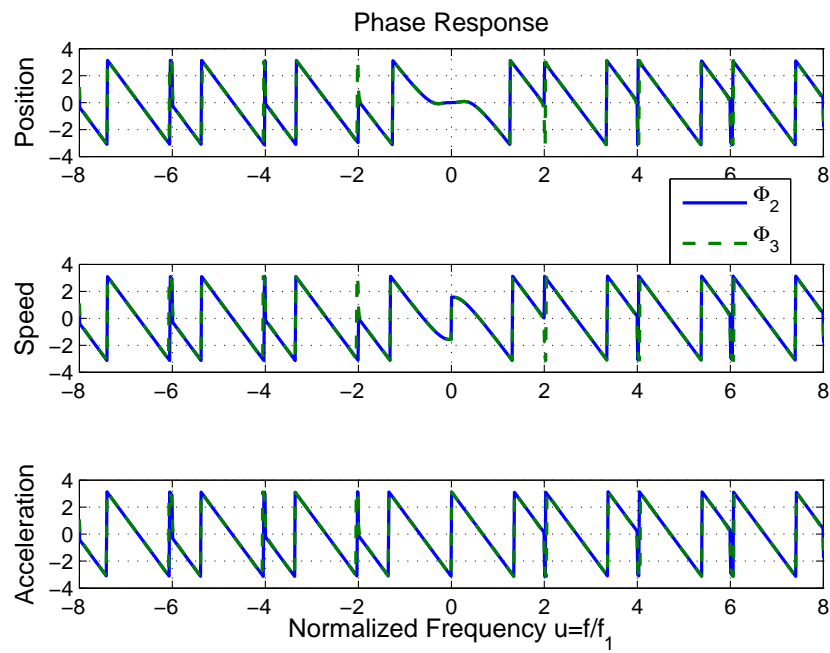


Figure 4.8: Phase response of the first three Taylor^K-Kalman-Fourier differentiators for $K = 2, 3$, and 32 harmonics. Close to the zero frequency, they have the ideal phase responses $(j\omega)$, and $(j\omega)^2$.

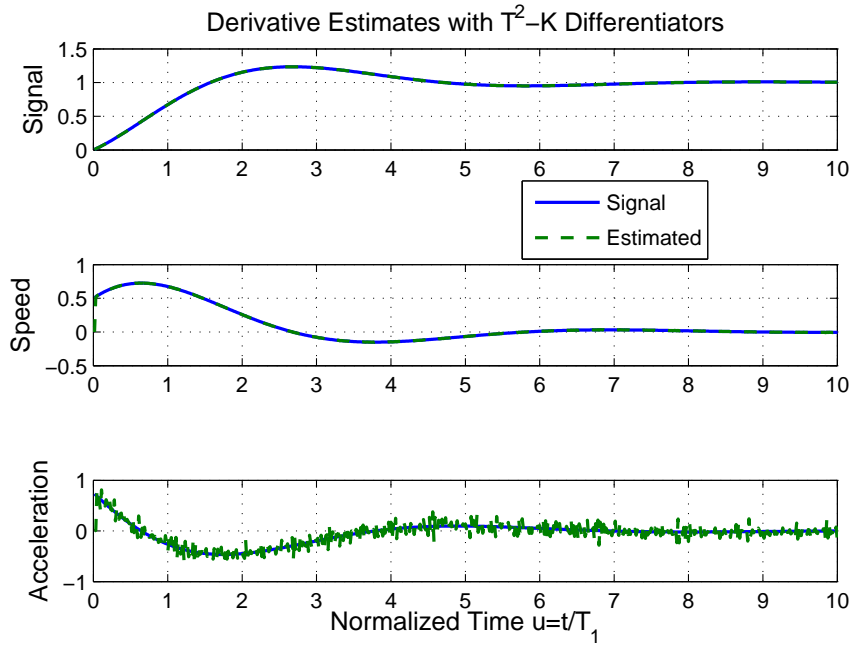


Figure 4.9: Signal, speed and acceleration estimates obtained with T^2 -K differentiators.

4.5 Numerical Results

In this section we test the T^K -K Differentiators with the following signal

$$s(t) = 1 - e^{-t/2} \cos(t) \quad (4.16)$$

sampled with $N_1 = 64$ samples per fundamental cycle. It is assumed that the signal is affected with additive white Gaussian noise (WGN) at the input of the state equations and at the output equation, with $\sigma_v^2 = 0.01$ and $\sigma_w^2 = 10^{-5}$ respectively. The results are obtained with the second and third T^K -K differentiators.

4.5.1 Taylor^K-Kalman Differentiators

The derivative estimates obtained with the second-order (T^2 -K) differentiators are shown in Fig. 4.9. It is apparent that the signal estimate and the first derivative are very close to the corresponding expected signals, but in the case of the acceleration estimates, noise is perceptible.

The estimates obtained with the T^3 -K differentiator are shown in Fig. 4.10. We can see that the acceleration estimates are quite improved. It is rare to see

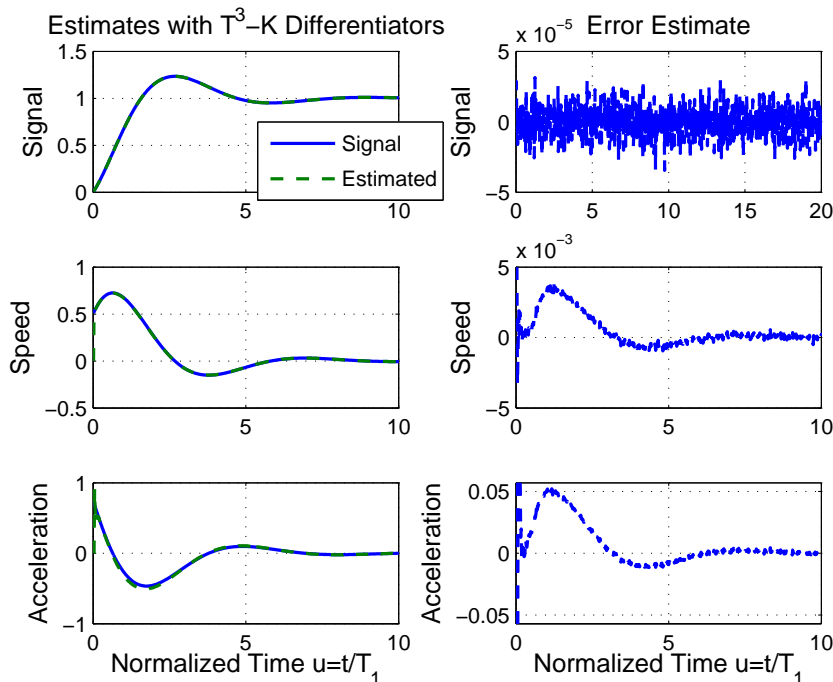


Figure 4.10: Signal, speed and acceleration estimates obtained with T^3 -K differentiators.

acceleration estimates as these. Derivatives estimated with finite difference equations are very sensitive to noise.

4.5.2 Low-Pass Taylor^K-Kalman Differentiators

The results obtained with the Low-Pass (LP) T^K -K differentiators are shown in Fig. 4.11 for $K=2$. It is apparent that they are better than those obtained without halfband gain mitigation. The estimates obtained with the LP T^3 -K differentiators are illustrated in Fig. 4.12. These differentiators can also obtain the third derivative, but they are not shown here.

4.5.3 Taylor^K-Kalman-Fourier Differentiators

Finally we present the estimates obtained with the T^K -K-F differentiators for $K = 2$ and 3, including 32 harmonics. The results are illustrated in Fig. 4.13. Note that they are very close each other. The transient at the beginning is due to the time needed to reach the permanent Kalman gains. It can be seen that the noise in the estimates has almost disappeared. It was observed that the transient response of

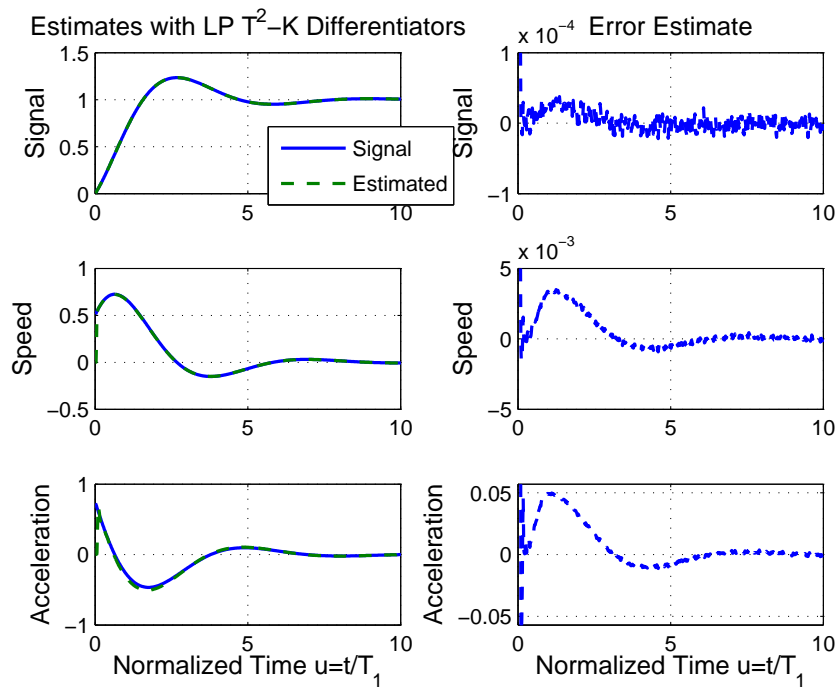


Figure 4.11: Derivative estimates obtained with the LP T^2 -K differentiators.

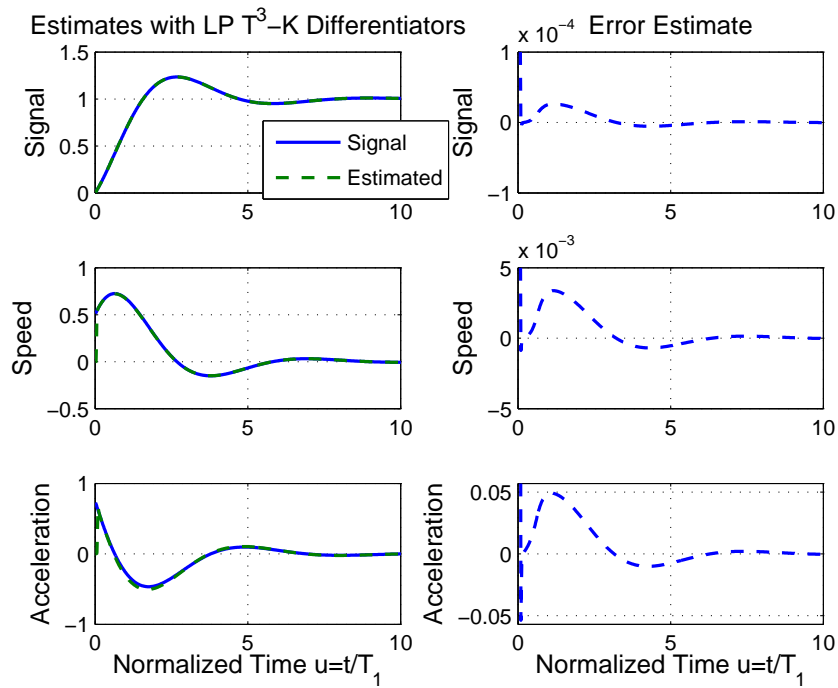


Figure 4.12: Derivative estimates obtained with the LP T^3 -K differentiators.

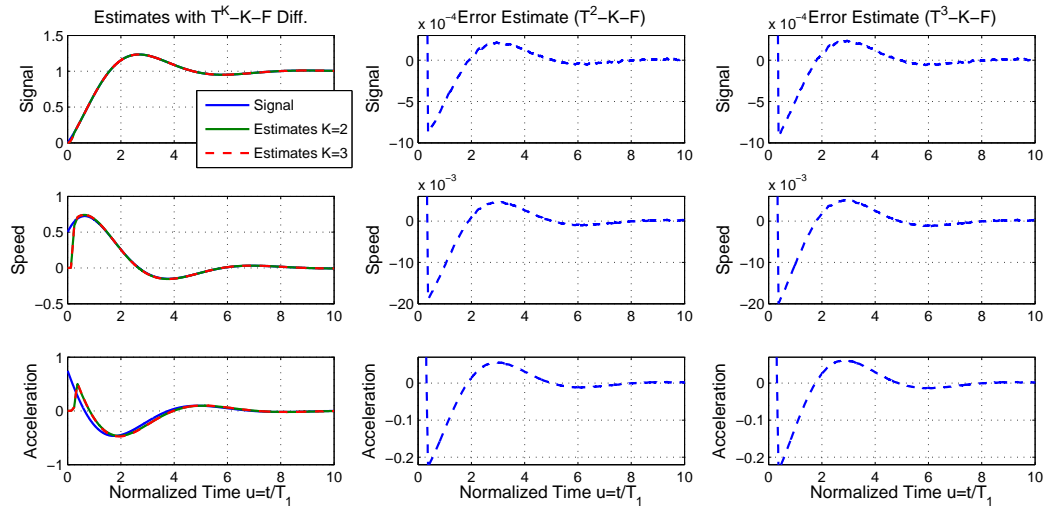


Figure 4.13: Derivative estimates obtained with the T^K -K-F differentiators for $K = 2, 3$ and including 32 harmonics.

the filters increases when more harmonics are included in the differentiators. Here we illustrated the derivatives of the zeroth harmonic, but this type of differentiators estimate the derivatives of the complex envelope of all the harmonic frequencies incorporated in the signal model. In the next example, we look at the derivatives of the complex envelope of the fundamental frequency.

4.5.4 Power Swing Signal Decomposed by T^2 -K-F Differentiators

Finally, the current signal of the power swing shown in the last example treated in [48] is taken again to illustrate the performance of the Kalman instantaneous differentiators. The Taylor²-Kalman-Fourier filter with harmonics $\{0, 1, 3, 5, 7\}$ was applied. The error of the signal approximation achieved by the Kalman filter is on the order of magnitude of -5 . Fig. 4.14 shows the amplitude and its derivative estimates. It corresponds to a real case of a current signal of a power swing in a European country (at 50Hz). The current signal is not shown. Note that the amplitude estimates have noise at the top of the crests, which is reflected in the corresponding derivative estimates. At the bottom, phase and its derivative (frequency) estimates are shown. Frequency in Hz was amplified four times to make it visible in that scale. The perceptible frequency offset is negative (-0.05Hz) because the system

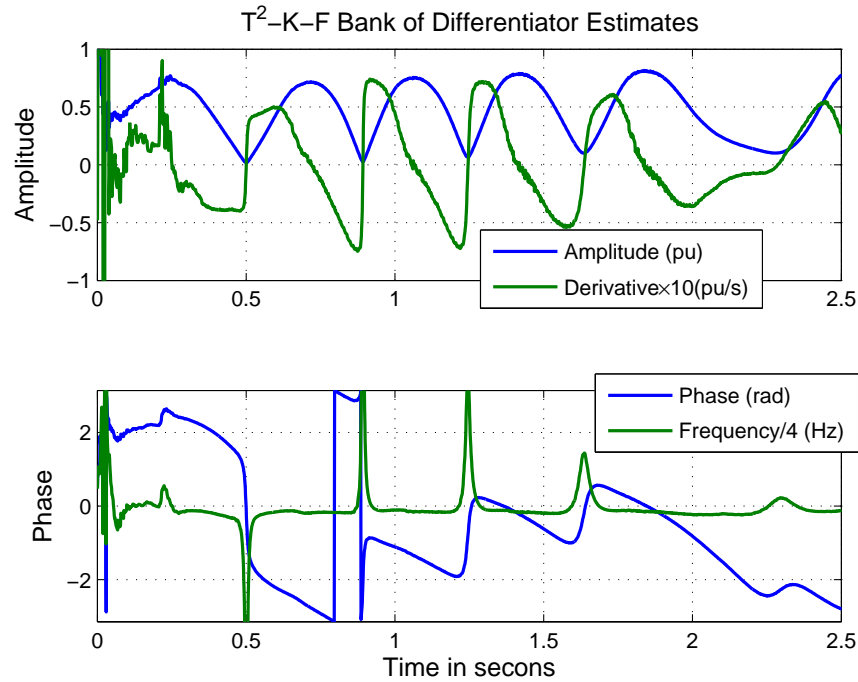


Figure 4.14: At the top, amplitude (continuous line) and derivative (dash line) instantaneous estimates of a swing current (in dots) in a power system at 50Hz. At the bottom, the instantaneous phase (continuous line) and frequency (dashed line) estimates of the same signal. Those estimates were obtained with the T^2 -K-F differentiators.

is overloaded. Abrupt changes in phase occur at zero amplitude instants, and are estimated by frequency (phase derivative) peaks. Note that amplitude and phase estimates are able to detect and measure the frequency peak occurring about 2.5s. In this case, we illustrate the estimates of the first harmonic, but they are available for the whole set of harmonics, So, the T^2 -K-F differentiators work as an extended spectrum analyzer of the signal.

4.6 Conclusions

Instantaneous derivative estimates were obtained with the T^K -K-F differentiators by applying the Kalman algorithm to a Taylor-Fourier signal model expressed in a state transition matrix. Several design possibilities were offered depending of the expected spectral load of the input signal. They perform as ideal differentiators with oscillating signals. Differentiator pass-bands and stop-bands can be adapted to the frequencies of interest, when they are known. They can be interpreted as an extension of the

DFT, and of the Taylor-Fourier transform, for $K > 0$, with much less computational burden than that of the FFT. They can be used as simple differentiators on the baseband, or as spectral analyzers of oscillating periodic signals, estimating not only the standard spectrum (amplitude and phase at each harmonic), but also their corresponding derivatives. In contrast to FFT, they provide instantaneous derivative estimates, very useful for control or synchronized monitoring applications.

Chapter 5

Conclusions

The new state transition matrices built with Taylor approximations to the dynamic phasor it is possible to obtain better instantaneous phasor estimates and its derivatives under oscillation conditions through the Taylor-Kalman-Fourier filter. The estimates achieved with the second order model reduce by a factor of ten the TVE error and are much more stable than those obtained with the traditional (zeroth-order) Kalman filter, with settling times five times lower. The extension of the signal model to the full set of harmonics was necessary to reduce the high noise sensitivity to the Taylor^K-Kalman filter. With the Taylor⁰-Kalman-Fourier filter it is possible to obtain the DFT Fourier coefficients of the signal. For orders greater or equal to two, the Taylor^K-Kalman-Fourier filters offer flat null phase response around harmonic frequencies. This means that their Fourier estimates are instantaneous (no delay at all). It is also possible to estimate the first derivatives of the oscillation. Finally, they can also be used as spectral analyzers of oscillating periodic signals.

The following conclusions can be drawn from the Taylor^K-Kalman filters: the Taylor signal model provides a state-transition matrix to model with better accuracy a power oscillation; a new technique for phasor estimation improves the phasor estimates of the traditional Kalman filter; the main advantage of the phasor estimates obtained with the T^K-K filter (for $K \geq 2$) is that they are instantaneous (no delay at all), preserving their synchrony with the signal, and with lower errors for oscillatory signals; finally, they reduce the computational cost as compared with the one cycle Fourier filter.

The following conclusions from the Taylor^K-Kalman-Fourier filters: By extending the signal model to the full set of harmonic frequencies, harmonic and noise rejection is improved; for $K = 0$, this filter bank obtains the DFT, but with

much less computational burden than the FFT; for $K \geq 0$, estimates of the complex envelope and its first derivatives can be estimated at every harmonic frequency, performing the Taylor-Fourier transform, when the spectrum of the input signal falls under the ideal differentiator gains; in the frequency domain, ideal differentiator gains are achieved around the harmonic frequencies, so when the spectral load of the input signal is confined in those bands, very good derivative estimates are achieved; finally, the new derivative estimates obtained with these filters are instantaneous (for $K \geq 2$) and therefore, good estimators of oscillating signals and their derivatives.

5.1 Contributions

The main contribution of the thesis is the dynamic signal model of the Taylor approximation to an oscillating signal. Before this contribution only static signal models existed. Better (instantaneous, more precise and fast) phasor estimates were achieved with the T^K -K filter. The T^K -K-F filter obtain instantaneous estimations for $K \geq 2$ with shorter transient times and improved the sensitivity to noise of the T^K -K filter. In addition to the phasor, they can estimate the first derivatives at each harmonic frequency. Spectral analysis can be done with those filters, obtaining instantaneous Fourier coefficients, and with much less computational burden as compared with the FFT algorithm.

5.2 Future Work

- To develop a new model for obtaining faster results when the signal has abrupt changes.
- Using the combination of gains obtained with Ackermann algorithm and the new kind of observers (using the Taylor^K-Kalman-Fourier Filters as observers) to obtain quicker estimates before abrupt changes.
- It was shown that it is possible to obtain the FFT with the Taylor-Kalman-Fourier filter, but it will be interesting to determine the advantages and disadvantages of these different methods.

Publications

- J. de la O, J. Rodríguez, “Instantaneous Dynamic Phasor Estimates with Kalman Filter”, in *Power and Energy Society General Meeting, 2010 IEEE*, 2010, pp. 1-6.
- J. de la O, J. Rodríguez-Maldonado, “Instantaneous Oscillating Phasor Estimates with Taylor^K-Kalman Filters”, in *IEEE Trans. Power Syst*, DOI:10.1109/TPWRS.2011.2157539, electronically available through IEEE Xplore.
- J. de la O, J. Rodríguez-Maldonado, “Frequency Response of Taylor^K-Kalman-Fourier filter for Instantaneous Oscillating Phasor Estimates”, in *IEEE Trans. Power Syst*, In Review.
- J. de la O, J. Rodríguez-Maldonado, “Taylor^K-Kalman-Fourier Differentiators for Instantaneous Derivative Estimates”, in *ELSEVIER*, Digital Signal Process., in Review.

Bibliography

- [1] H. W. Sorenson, "Least-squares estimation: from Gauss to Kalman," *IEEE Spectr.*, vol. 7, no. 7, pp. 63–68, 1970.
- [2] A. Girgis and R. Brown, "Application of Kalman filtering in computer relaying," *IEEE Trans. Power App. Syst.*, vol. 100, no. 7, 1981.
- [3] J. S. A. Girgis and E. Makram, "Measurement and prediction of voltage flicker magnitude and frequency," *IEEE Trans. Power Del.*, vol. 10, no. 3, pp. 1600–1605, 1995.
- [4] D. Hart and A. Girgis, "Application of Kalman filtering on a vector signal processor," *Proceedings., Twenty-Third Southeastern Symposium on*, pp. 399–403, 1991.
- [5] W. B. C. Adly, A. Girgis and E. B. Makram, "A digital recursive measurement scheme for on-line tracking of power system harmonics," *IEEE Trans. Power Del.*, pp. 1153–1160, 1991.
- [6] ———, "Analysis of high-impedance fault generated signals using a Kalman filtering approach," *IEEE Trans. Power Del.*, pp. 1714–1724, 1990.
- [7] A. A. Girgis, "A new Kalman filtering based digital distance relay," *IEEE Trans. Power App. Syst.*, pp. 3471–3480, 1982.
- [8] H. C. W. M. S. Sachdev and N. G. Johnson, "Kalman filtering applied to power system measurements for relaying," *IEEE Trans. Power App. Syst.*, pp. 3565–3573, 1985.
- [9] "Standard for synchrophasors for power systems," *IEEE Std. C37.118-2005*.

- [10] K. Martin, D. Hamai, M. Adamiak, S. Anderson, M. Begovic, G. Benmouyal, G. Brunello, J. Burger, J. Cai, B. Dickerson, V. Gharpure, B. Kennedy, D. Karlsson, A. Phadke, J. Salj, V. Skendzic, J. Sperr, Y. Song, C. Huntley, B. Kasztenny, and E. Price, "Exploring the iee standard c37.118-2005 synchrophasors for power systems," vol. 23, no. 4, pp. 1805–1811, 2008.
- [11] A. G. Phadke and J. S. Thorp, *Computer Relaying for Power Systems*, 1st ed. Research Studies Press LTD, Sep. 1988.
- [12] L. Salvatore and A. Trotta, "Flat-top windows for PWM waveform processing via DFT," *Electric Power Applications, IEE Proceedings B*, vol. 135, no. 6, pp. 346–361, 1988.
- [13] J. de la O Serna and K. Martin, "Improving phasor measurements under power system oscillations," *IEEE Trans. Power Syst.*, vol. 18, no. 1, pp. 160–166, 2003.
- [14] W. Premerlani, B. Kasztenny, and M. Adamiak, "Development and implementation of a synchrophasor estimator capable of measurements under dynamic conditions," *Power Delivery, IEEE Transactions on*, vol. 23, no. 1, pp. 109–123, 2008.
- [15] D. Fan and V. Centeno, "Phasor-Based synchronized frequency measurement in power systems," *IEEE Trans. Power Del.*, vol. 22, no. 4, pp. 2010–2016, 2007.
- [16] A. Phadke and B. Kasztenny, "Synchronized phasor and frequency measurement under transient conditions," *IEEE Trans. Power Del.*, vol. 24, no. 1, pp. 89–95, 2009.
- [17] P. Mattavelli, A. Stankovic, and G. Verghese, "SSR analysis with dynamic phasor model of thyristor-controlled series capacitor," *IEEE Trans. Power Syst.*, vol. 14, no. 1, pp. 200–208, 1999.
- [18] S. S. S. Dambhare and M. Chandorkar, "Adaptive current differential protection schemes for transmission-line protection," *Energy Society General Meeting, 2010 IEEE*.
- [19] J. de la O Serna, "Dynamic phasor estimates for power system oscillations," *IEEE Trans. Instrum. Meas.*, vol. 56, no. 5, pp. 1648–1657, october 2007.

- [20] M. A. Platas and J. A. de la O Serna, "Dynamic phasor and frequency estimates through maximally flat differentiators," *IEEE Trans. Instrum. Meas.*, vol. 59, no. 2, april 2010.
- [21] ———, "Dynamic harmonic analysis through taylor-fourier transform," *IEEE Trans. Instrum. Meas.*, vol. 60, no. 3, pp. 804–813, march 2011.
- [22] A. Girgis and R. Brown, "Application of Kalman filtering in computer relaying," *IEEE Trans. Power App. Syst.*, vol. 100, no. 7, pp. 3387–3397, Jul. 1981.
- [23] A. Girgis, "A new Kalman filtering based digital distance relay," *IEEE Trans. Power App. Syst.*, vol. 101, no. 9, pp. 3471–3480, 1982.
- [24] W. H.C., N. Johnson, and M. Sachdev, "Kalman filtering applied to power system measurements relaying," *Power Apparatus and Systems, IEEE Transactions on*, vol. 104, no. 12, pp. 3565–3573, 1985.
- [25] J. P. de Sa, "A new Kalman filter approach to digital relaying," *IEEE Trans. Power Del.*, vol. 7, no. 3, pp. 1652–1660, 1992.
- [26] L. Wang, "Frequency responses of phasor-based microprocessor relaying algorithms," *IEEE Trans. Power Del.*, vol. 14, 1999.
- [27] P. K. Dash, R. K. Jena, G. Panda, and A. Routray, "An extended complex Kalman filter for frequency measurement of signals," *IEEE Trans. Instrum. Meas.*, vol. 49, 2000.
- [28] P. Zarchan, H. Musoff, and F. K. Lu, *Fundamentals of Kalman Filtering: A Practical Approach*, 3rd ed. AIAA (American Institute of Aeronautics & Ast, Sep. 2009.
- [29] D. G. Manolakis, D. Manolakis, V. K. Ingle, and S. M. Kogon, *Statistical and Adaptive Signal Processing: Spectral Estimation, Signal Modeling, Adaptive Filtering and Array Processing*. Artech House Publishers, Apr. 2005.
- [30] D. Simon, *Optimal State Estimation: Kalman, H Infinity, and Nonlinear Approaches*. Wiley-Interscience, Jun. 2006.
- [31] S. J. R. D. A. C. Max A. Little, Patrick E. McSharry and I. M. Moroz., "Exploiting nonlinear recurrence and fractal scaling properties for voice disorder detection," *Biomed Eng. Online*, vol. 6, no. 23, 2007.

- [32] J. A. de la O Serna and J. Rodriguez, “Instantaneous dynamic phasor estimates with Kalman filter,” in *IEEE PES General Meeting*, 2010.
- [33] J. A. de la O Serna and J. Rodriguez-Maldonado, “Instantaneous oscillating phasor estimates with Taylor^k-Kalman filters,” *IEEE Trans. Power Syst.*
- [34] L. Wang, “Frequency responses of phasor-based microprocessor relaying algorithms,” *IEEE Trans. Power Del.*, vol. 14, no. 1, pp. 98 – 109, January 1999.
- [35] G. Benmouyal, “Frequency-domain characterization of Kalman filters as applied to power system protection,” *IEEE Trans. Power Del.*, vol. 7, no. 3, pp. 1129–1138, 1992.
- [36] R. Haeb-Umbach and M. Bevermeier, “OFDM channel estimation based on combined estimation in time and frequency domain,” in *Acoustics, Speech and Signal Processing, 2007. ICASSP 2007. IEEE International Conference on*, vol. 3, 2007, pp. 277–280.
- [37] Z. Cheng and D. Dahlhaus, “Time versus frequency domain channel tracking using Kalman filters for OFDM systems with antenna arrays,” in *Vehicular Technology Conference, 2003. VTC 2003-Spring. The 57th IEEE Semiannual*, vol. 1, 2003, pp. 651–655.
- [38] F. Cornett, “Kalman estimation of frequency-domain interference reduction coefficients for angle-modulated signals,” in *Acoustics, Speech, and Signal Processing, IEEE International Conference on ICASSP '84.*, vol. 9, 1984, pp. 290–293.
- [39] S. Cooper and H. Durrant-Whyte, “A frequency response method for multi-sensor high-speed navigation systems,” in *Multisensor Fusion and Integration for Intelligent Systems, 1994. IEEE International Conference on MFI '94.*, 1994, pp. 1–8.
- [40] M. A. Platas Garza and J. A. de la O Serna, “Dynamic phasor estimates through maximally flat differentiators,” in *2008 IEEE Power and Energy Society General Meeting - Conversion and Delivery of Electrical Energy in the 21st Century*. IEEE, Jul. 2008, pp. 1–8.

- [41] M. A. Al Alaoui, "Direct approach to image edge detection using differentiators," in *2010 17th IEEE International Conference on Electronics, Circuits, and Systems (ICECS)*. IEEE, Dec. 2010, pp. 154–157.
- [42] M. A. Platas-Garza and J. A. de la O Serna, "Dynamic phasor and frequency estimates through maximally flat differentiators," *IEEE Transactions on Instrumentation and Measurement*, vol. 59, no. 7, pp. 1803–1811, Jul. 2010.
- [43] S. Manchanda and P. Rastgoufard, "Utilization of extrapolated integrators and differentiators in digital controller design and analysis," in *IEEE Southeastcon '90. Proceedings*. IEEE, Apr. 1990, pp. 906–910 vol.3.
- [44] S. Ibrir, "New differentiators for control and observation applications," in *American Control Conference, 2001. Proceedings of the 2001*, vol. 3. IEEE, 2001, pp. 2522–2527 vol.3.
- [45] Y. X. Su, C. H. Zheng, D. Sun, and B. Y. Duan, "An enhanced fuzzy PD controller with two discrete nonlinear tracking differentiators," *Control Theory and Applications, IEE Proceedings -*, vol. 151, no. 6, pp. 675–682, Nov. 2004.
- [46] J. G. Proakis and D. G. Manolakis, *Digital Signal Processing*, 4th ed. New Jersey: Prentice Hall, 2007.
- [47] T. W. Parks and J. H. McClellan, "Chebyshev approximation for nonrecursive digital filters with linear phase," *IEEE Trans. Circuit Theory*, vol. 19, pp. 189–194, 1972.
- [48] J. A. de la O Serna and M. A. Platas-Garza, "Maximally flat differentiators through wls taylor decomposition," *Elsevier Digital Signal Processing*, vol. 21, no. 2, pp. 183–194, 2011.
- [49] I. Selesnick, "Maximally flat low-pass digital differentiators," *IEEE Trans. Circuits Syst. II*, vol. 49, no. 3, pp. 219–223, 2002.
- [50] B. Carlsson, "Maximum flat digital differentiator," *Electron. Lett*, vol. 27, no. 8, pp. 675–677, 1991.
- [51] I. R. Khan and R. Ohba, "New design of full band differentiators based on taylor series," *Proc. Inst. Elect. Eng. Visual Image Signal Process*, vol. 146.

- [52] B. Kumar and S. C. D. Roy, "Design of universal variable frequency range fir digital differentiators," *Circuits Systems signal Processing*, vol. 11, no. 3, 1992.
- [53] ———, "Maximally linear fir digital differentiators for midband frequencies," *Int. J. Circuit Theory Appl.*, vol. 17, no. 1, pp. 21–27, 1989.
- [54] B. Kumar and S. C. . D. Roy, "Design of digital differentiators for low frequencies," *Proc. IEEE*, vol. 76, no. 3, pp. 287–289, 1988.
- [55] E. Hermanowicz, "Designing linear-phase digital differentiators a novel approach," *European Signal Processing, 14th EUSIPCO Conference on.*
- [56] S. C. D. Roy and B. Kumar, "On digital differentiators, hilbert transformers, and half-band low-pass filters," *IEEE Trans. Educ.*, vol. 32, no. 3, 1989.
- [57] X. Zhang and T. Yoshikawa, "Design of full band iir digitla differentiators," *IEEE Trans. Neural Netw.*, vol. 1.
- [58] M. A. Al-Alaoui, "Linear phase Low-Pass IIR digital differentiators," *IEEE Trans. Signal Process.*, vol. 55, no. 2, 2007.
- [59] J. B. Moore, "Optimum differentiation using Kalman filter theory," *IEEE Proceedings Letters*, vol. 56, no. 5, p. 871, 1968.